1975

I. Precision Measurements With a Ruby Laser. II. A Quantum Mechanical Paradox.

Rory Oliver Rice
Louisiana State University and Agricultural & Mechanical College

I. PRECISION MEASUREMENTS WITH A RUBY LASER

II. A QUANTUM MECHANICAL PARADOX

A Dissertation

Submitted to the Graduate Faculty of the
Louisiana State University and
Agricultural and Mechanical College
in partial fulfillment of the
requirements for the degree of
Doctor of Philosophy

in

The Department of Chemistry

By
Rory Oliver Rice
B.S., Louisiana State University, 1968
May, 1975

TABLE OF CONTENTS

TABLES

FIGURES

PROLOGUE

This dissertation consists of two parts: Part I, Precision Measurements with a Ruby Laser; and Part II, A Quantum Mechanical Paradox. The two parts represent the results of two non-related areas of study by myself while a graduate student. My attention was directed primarily to a study of photographic emulsion blackening produced by high power laser pulses. At one point a prolonged equipment failure halted progress in Part I. During this time I did the work described in Part II. The topic of Part II was suggested to me by my major professor, Dr. James D. Macomber, who ran across the problem while teaching a course.

Rory O. Rice

ABSTRACT: PART I

In attempting to make precise spectroscopic measurements with a ruby laser, many problems can arise which will negate the value of the data obtained. Part I of this paper discusses many of these problems and how to eliminate them. Then the results are applied to a simple experiment, that of measuring high intensity reciprocity failure in photographic emulsions. Furthermore, it is shown that one can use a photographic emulsion in place of a photodetector for making accurate and precise measurements.

ABSTRACT: PART II

Part II of this paper is a comparison of classical and quantum mechanics in relation to the Uncertainty Principle. It is demonstrated that in a statistical examination of a large number (e.g., 10^{23}) of particles, classical mechanics also has an "uncertainty principle" and that in fact the classical uncertainty may be greater than the quantum uncertainty.

PART I -- CHAPTER I

PRECISION MEASUREMENTS WITH A RUBY LASER

Anyone who desires to obtain precise results from an experiment in which a pulsed laser is employed as the light source faces many difficulties. The research described in this dissertation was undertaken to overcome as many of these difficulties as possible. The potential utility of pulsed lasers that justifies this effort is due to characteristics of a typical pulse: brevity (10^{-8}s); power (10^{8} watts); and monochromaticity (band width ~10^{9}Hz). By way of contrast, typical continuous lasers have powers which range from 10^{-4} to 10^{-2} watts and band widths in the range of 10^{7}Hz. In this study we shall have in mind a particular class of experiments using the pulsed laser--a spectroscopic study of the non-linear optical behavior of matter. Pulsed lasers must be used because non-linear optical effects produced by conventional light sources (or even continuous lasers) are unobservably small in most cases.

The advent of lasers with their unique beam characteristics has presented the chemist with opportunities to learn more about the properties of matter. Continuous wave (c.w.) lasers presented few engineering problems in using them for spectroscopic experiments. The new laser Raman spectrophotometers enable chemists to make more detailed studies of matter, and have already become almost as easy to use as conventional infrared spectrophotometers.

In contrast to c.w. radiation, modern spectroscopic tools and methods are not readily adapted to high-intensity short-duration bursts of energy. Therefore it is not nearly so easy to make accurate and precise spectroscopic measurements with pulsed lasers. However, the need for such measurements is present, since such measurements are necessary for studying proposed theories dealing with non-linear optical phenomena. Measurements taken with pulsed lasers typically have statistical uncertainties of 100%. Clearly very little can be done with such imprecise data.

In this paper, many of the difficulties encountered in making precision measurements with a pulsed laser are examined. Consideration must be given to whether or not the special characteristics of pulsed laser beams might cause various components used in detection systems to behave differently from those used with conventional light sources. After suggesting solutions to these problems, an example of a precision measurement will be presented.

The pulsed laser available for this work was an Optics Technology model 130 (serial #130) ruby laser. A schematic diagram of the laser head is shown in Fig. 1.

The source of the laser beam is a pink ruby rod (R) approximately 3/8" diameter and 3" long. The ruby is pumped by two parallel linear flash lamps (F). The reflectors M and P cause the light to make multiple passes through the ruby, thus increasing the effective path length through the amplifying medium without increasing the length of the rod.

Metallic and dielectric mirrors are not used as reflectors because they absorb part of the incident light. If even a small fraction of the extremely intense light produced within the laser cavity were absorbed, the absorbing material would quickly vaporize due to the high temperatures. Thus holes would be burned in such mirrors and the laser would cease to operate after a few firings. In the case of the model 130 laser, a 90° prism (P) is used as the rear reflector, producing almost 100% reflection; as long as the front surface is kept clean and free of dust, there will be a negligible amount of absorption. The front reflector is a transparent sapphire flat (M); however, its index of refraction ($n=1.763$)[1] is high enough to produce a high reflectivity for some of the light which strikes it. The total reflectance of the flat is an oscillating function of wavelength and ranges from zero to 0.26. The reflectance is a maximum of $\left(\frac{1 - n^2}{1 + n^2}\right)^2$ if

$$2t = (m + 1/2)\lambda$$

where t is the thickness of the flat, m an integer, and λ the wavelength of the light inside the flat.[2] The reflectance is zero if

$$2t = m\lambda$$

Therefore not only does the flat act as a reflector but it also serves as a wavelength selector permitting feedback (and therefore gain) for a narrower spectral distribution within the laser.

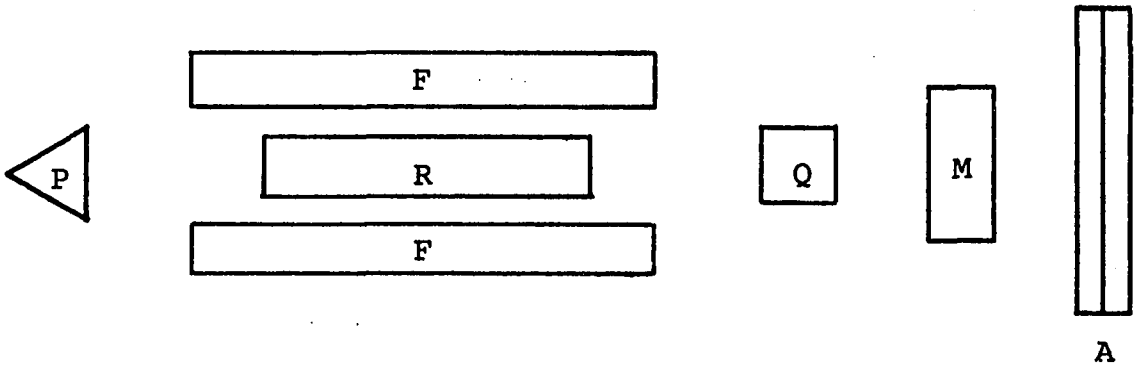

Figure 1

Ruby Laser Schematic

A laser with the above components (ruby rod, flash lamps, and reflectors), when pumped to its threshold (i.e., when just enough energy is pumped into the ruby rod by means of a single flash from the lamps to cause it to fire) should produce a single pulse with a duration of a few microseconds. However, if pumped slightly over threshold it will fire more than one pulse and if slightly under threshold it will not fire at all. In the case of the model 130 ruby laser it seems to be nearly impossible to pump the ruby exactly to threshold. Using a pump energy which is experimentally determined to be close to the threshold seems to produce multiple pulses about half the time and no pulses the other half. Clearly, to have no pulses at all is undesirable, but one might ask what is undesirable about two pulses. Perhaps in some experiments it would make no difference as long as every pulse produced were detected. This in itself is a problem, however, which will be discussed in detail later. On the other hand there are many experiments in which two pulses, not necessarily of equal intensity or duration and not always the same time interval apart, would make interpretation of the results very difficult.

A Q-switch (Q) introduced into the laser, prevents the laser from firing a single pulse until it is pumped an amount ΔE_1 above the non-Q-switched threshold E_o. The magnitude of ΔE_1 can be adjusted by changing some property of the Q-switch. This has the effect of raising the laser threshold and, what might be called the multiple pulse threshold, $E_o + \Delta E_m$ even

more. The term multiple pulse threshold is used here to designate the pump energy at which the laser fires more than once. The result of this is that there exists a range of pump energies, E, which give a single pulse for each setting of the Q-switch. In particular the range is $E_o + \Delta E_1 \leq E \leq E_o + \Delta E_m$. Another more dramatic effect of the Q-switch is to shorten the duration of the pulse and increase the peak power by several orders of magnitude. There are many methods of Q-switching available: electro-optic modulators, mechanical modulators, magneto-optic modulators, acoustic-wave modulators, and saturable barriers.[3]

A saturable barrier consisting of a dilute solution of cryptocyanine[4] dye in methanol was used in this work. Cryptocyanine (which has an absorption band at 706 nm) absorbs the red light (694.3 nm) produced by the ruby, preventing that light from reaching the front mirror M and thereby preventing laser action. The dye continues to absorb the ruby luminescence until it absorbs so much energy that it saturates. When saturation occurs, the dye becomes transparent and allows the red light to pass through and the laser to fire. This method of Q-switching has disadvantages, however. In the discussion just given, it is assumed that the saturation is reversible; when the red light intensity decreases the cryptocyanine returns, with no decomposition, to its ground state. Unfortunately, the flash lamps produce large amounts of ultraviolet light in addition to the visible which rapidly breaks down the dye photochemically, decreasing its optical

density. Each fresh Q-switch solution is rendered ineffective after only a few uses. This problem has been studied by Hollier and Macomber;[5] they have shown that the problem can be reduced considerably by using Pyrex containers rather than quartz. Although the same authors[6] have shown that the additional precaution of removing oxygen from the sample will eliminate the decomposition completely, glass cells alone stabilized the dye sufficiently for the work to be reported here.

The monochromatic red laser light emerging from the laser aperture is unfortunately accompanied by the white light, at lower power but of longer duration than the laser pulse(s), from the flash lamps. This may be reduced to a negligible amount by placing in front of the reflector (M) two Corning number 2-58 cut-off filters (A) which absorb almost all of the light of wavelengths shorter than 600 nm.[7] The components of the laser head displayed in Fig. 1 are mounted in a cabinet having a small circular aperture between the front mirror M and the Corning filters A, so that all of the flash lamp light leaving the laser cavity strikes the filter.

COLLIMATION OF THE BEAM

The problems inherent within the laser itself have been described and suggestions for eliminating these problems were proposed. Now the laser beam must be examined to determine what difficulties could arise from its characteristics. It is well-known that the divergence of laser beams

is supposed to be very small. But this characteristic is really attributed accurately only to c.w. lasers. Pulsed lasers, although they do have a beam divergence considerably narrower than that of a flashlight, usually have substantially more divergent beams than those of c.w. lasers. Also c.w. lasers can be made to produce beams with a Gaussian intensity distribution in the direction perpendicular to the beam, with the center of this distribution on the axis of the laser tube. The OTI 130 ruby laser does not usually behave so nicely. It tends to fire in "filaments" which are smaller than the face of the rod, seldom on the axis of the rod or from any other particular point on its face. Multiple firings of $\underline{n}$ pulses are from $\underline{m}$ such filaments, $\underline{m} \leq \underline{n}$. Finally, since a ruby rod has a rather large cross-section in comparison to its length, it is possible for the pulse to be directed at an off-axis angle. Pulsed lasers are such high-gain devices that the light in the laser cavity requires only a few passes through the rod in order to achieve the laser threshold intensity; therefore a slightly off-axis angle pulse may gain enough energy to lase before it "walks off" the cylinder of the ruby rod. (An ideal laser is one which, in effect, needs an infinite number of bounces to "lase". The slightest angular error will be magnified to walkoff.) It is thus clear that because the beam characteristics of a pulsed laser are not nearly so nice as those from a c.w. laser, considerable care must be taken to see that those characteristics do not affect the data. One thing that may be done to alleviate

the worst consequences of those effects is to use a pair of apertures on the axis of the laser. One might think at first that pinhole sized apertures should be used, so that the beam would always be parallel and on the optic axis; however, if this were actually done, very few rays from the laser beams would get past the apertures. In addition, if pinholes of diameter less than or nearly equal to the laser wavelength are used, diffraction effects would cause the beam divergence to worsen rather than improve. Therefore a compromise must be reached between pinhole apertures and the absence of apertures. The apertures used in this work were both 0.833 ± 0.003 cm in diameter and 90.0 ± 0.3 cm apart. This eliminated rays from laser pulses fired from filaments which depart greatly from the optic axis by placing limits on the detection angles, i.e., the maximum divergent angles which are allowed to pass through the apertures and strike a detector surface.

PULSE COUNTING

One more problem previously mentioned is this: did the laser fire one pulse or more than one? Attempts were made to answer this question by reflecting a small fraction of each laser pulse from a glass flat into a photoelectric detector. The detector was monitored by an oscilloscope set on a relatively slow sweep rate. Ideally every pulse from a laser shot would produce a "spike" on the oscilloscope. One spike meant one pulse as desired, and n spikes meant n pulses and such a shot was discarded. (One "shot" means one firing

of the xenon flashlamps used to pump the laser. The duration of one shot is of the order of 10^{-3} s.) The detector was a TRG model 105B photodetector (serial #213-6) with an S-1 surface. The photodetector was powered by a John Fluke model 405 power supply (serial #123) at 2000 volts, and the output signal from the detector was fed into a Tektronix 535 oscilloscope (serial #3350). Photographs were taken of the oscilloscope traces with a Tektronix model C-31 polaroid camera (serial #B20201). The sweep rate of the oscilloscope was set on a "slow" sweep rate of between 5 and 25 μs/division, depending on the dye concentration used in the Q-switch. Lower dye concentrations require longer scans. This "pulse counting system" worked well for high powered short pulses most of the time; however, it worked very poorly for the low-powered, longer pulses. The system was pushed to its maximum sensitivity in the latter case and sometimes there simply was not enough power to trigger the oscilloscope.

Sometimes the laser produced a very weak pulse followed by a stronger pulse. It became evident that many times in such cases the oscilloscope was not triggered by the first pulse but by the second. The inverse order is easily detected since once the oscilloscope is triggered by a strong pulse, very weak pulses show up as a small "blip" on the trace. The problem of course is that it was frequently not possible to determine with certainty whether a detector registered one pulse or more than one. Also for some reason which could not be determined by the author, the oscilloscope sometimes was not triggered by pulses which evidently had

more than enough power to do so. This problem occurred throughout the course of experimentation. Note that neither the glass flat nor filters placed between the laser and photodetector must have calibrated or quantitatively reproducible absorbances, and this allows lower quality components to be used.

ENERGY MEASUREMENT

In order to make many quantitative measurements, it is necessary to know the total output energy of the laser pulse. The detector most frequently used for this purpose was a Korad model KJ-2 calorimeter (serial #220-3353-6). A large fraction of the pulse (~95%) is reflected into the calorimeter by a partially-transmitting dielectric reflector. Even though the energy may be measured with the calorimeter, it is far from ideal for this purpose. This is partly because a calorimeter does nothing but measure energy and partly because it is extremely insensitive: 95% of a high powered laser pulse is barely sufficient to cause it to produce a weak signal.

Red laser light entering the aperture of the calorimeter is absorbed by a blue solution of copper sulfate. When the light is absorbed, the small volume of liquid undergoes a slight increase in temperature, which then produces a potential difference in a thermocouple. A typical 0.1 joule pulse generates a two microvolt change in the thermocouple voltage, which was measured with a Keithley model 150A microvolt-ammeter (serial #44-918). Thermal fluctuations in

the room and line voltage fluctuations can have a considerable effect on this energy-measurement system. The room temperature is held to 20° ± 2°C when the air conditioning system is functioning. However, drafts from opening the door to the hall outside of the laboratory can cause changes of several microvolts. Many layers of insulating material were wrapped around the calorimeter to lessen such effects. Even though the Keithley is designed to handle changes in line voltage, its behavior was considerably improved by interposing between it and the line source a constant voltage regulating system consisting of a Sola constant voltage transformer (catalog #30807 and serial #D511) and a Powerstat voltage regulator (type 116 and LSU serial #306720). Also, an Esterline Angus minigraph recorder model M11A01B4-000 (serial AK71) was used to record the voltage from the Keithley microvoltmeter. Despite all of these precautions (which usually made the Keithley as "steady as a rock"), there were some days in which this system was so unstable as to be impossible to use. The reason for this instability was never discovered.

In spite of the instability of the calorimeter energy-measurement system and the fact that it required almost all of the laser pulse to use it, its operation is so straightforward that it was never replaced as the primary standard for all of the other detectors. For increased convenience in use, photoelectric detectors (calibrated using the calorimeter by means of a procedure to be described shortly) were

employed in almost every experiment.

An optics Technology Inc. model 620 ultra fast photodiode detector with an S-20 surface (serial #140-20) was one of two such photoelectric devices. (The TRG photodetector previously mentioned was initially used for this purpose, but because of its lower sensitivity it was later used only for pulse counting.) When the internal power supply of the OTI burned out and replacement parts were no longer available, four 510 volt electronic flash batteries (available from any photographic supply store) were used to supply the high voltage. The amplitude of the output signal from the photodetector versus time was displayed on the screen of a Tektronix 519 oscilloscope (serial #000999), and the traces were recorded on polaroid film in a Tektronix C-27 camera (serial #002757). The photodetector has the advantages that it is several orders of magnitude more sensitive than the calorimeter, and it also gives more information (i.e., pulse width and shape and even peak power). Because it was uncalibrated and not reproducible, it was necessary to calibrate the photodetector against the calorimeter. Always, enough sensitivity data were gathered so that the statistical mean could be taken as an accurate indicator of its true value. A typical pulse recorded from the photodetector is shown in Fig. 2. Note the x-axis deflection is proportional to the time (in nanoseconds) and the y-axis deflection is driven by the signal from the photodetector (in volts). The latter, in turn, is proportional to the light intensity (in watts). The pulse

width is taken as the full width at 1/2 the peak height. The energy of the pulse is proportional to the area under the trace. Calibration of the photodetector gives the necessary constants of proportionality to convert volts into watts and volt · ns into joules. A schematic of the experimental setup finally used for this photodetector calibration is shown in Fig. 3. Several more unusual arrangements were tried, first in the attempt to make more efficient use of each laser shot, and second in the attempt to eliminate many problems of data reproducibility. Some of these arrangements will be discussed in this paper as each problem encountered will be examined.

The first calibration attempt was performed with the most obvious arrangement, shown in Fig. 4. The experiment seemed to be trivially easy: fire the laser directly into the calorimeter, reflecting a small fraction of the pulse from a glass flat into the photodetector to be calibrated. Varying the pump energy of each laser shot and gathering data from 30 to 40 shots should be sufficient to overcome the effects of statistical fluctuations in the photodetector performance. A plot of oscillogram trace area versus calorimeter energy should be a straight line through the origin. The areas of the oscillograms were measured with a Lasico compensating polar planimeter model #123A (serial #5745). Each oscillogram was measured ten times with the mean accepted as the true measure of the area. It is desirable to have the calibration data extend over as many orders of magnitude of incident energy as possible. Since the Tektronix 519 has no

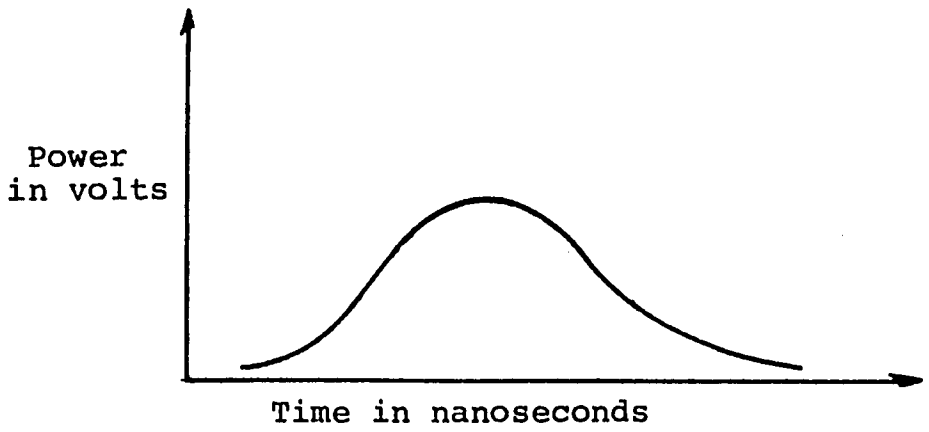

Figure 2

Typical Laser Pulse

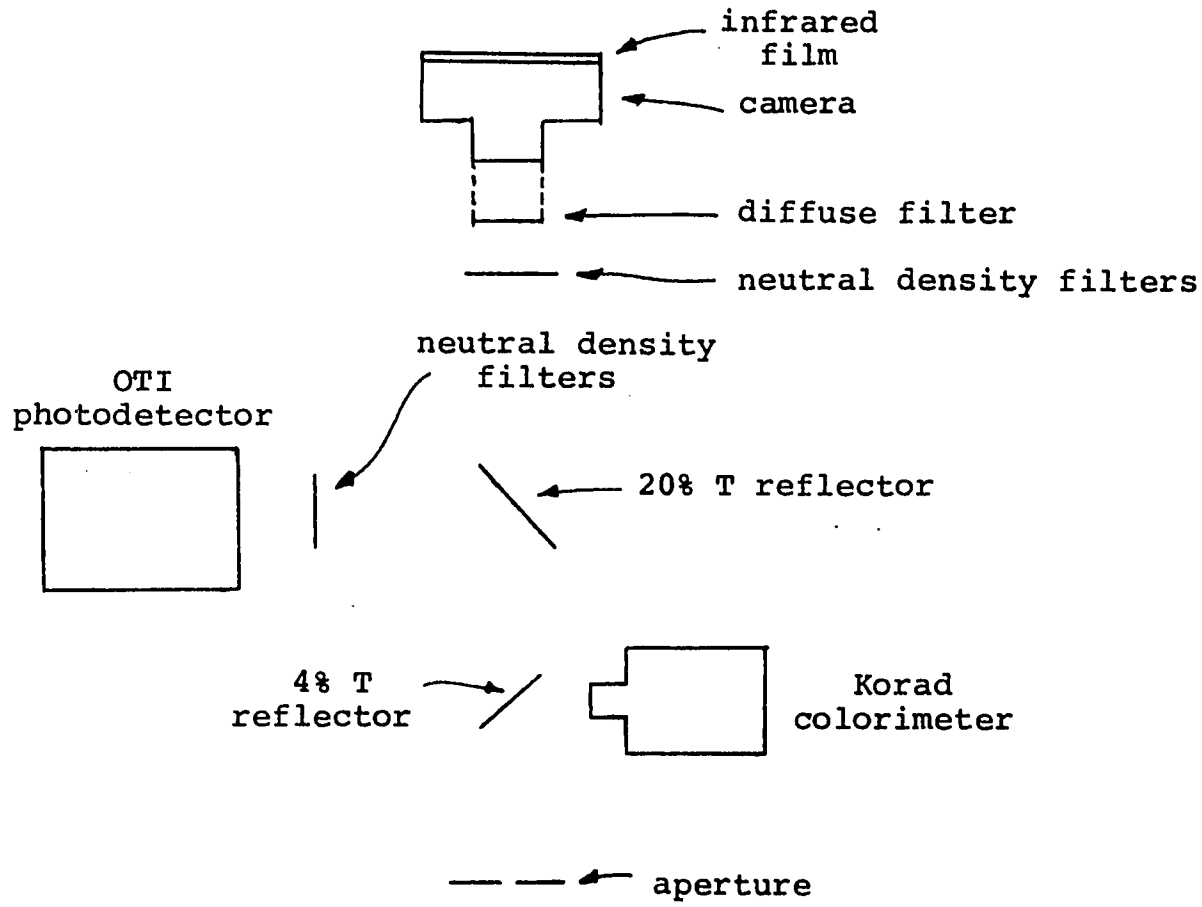

Figure 3

Final Arrangement of Apparatus

y-axis amplifier (because such amplifiers produce pulse distortion), only pulses of from 2 to 20 volts amplitude are measurable, and the most precise results were obtained from those between 10 and 20 volts. This feature of the photodetector system limits measurement capability to less than one order of magnitude unless the signal from the photodetector can be amplified or attenuated linearly and reproducibly. As was mentioned, amplification is not desirable since it leads to peak distortion, a very undesirable trait in quantitative measurements. (The usual benefit of amplification, increase in signal size, is really not necessary here because of the high sensitivity of the photodetectors.) Therefore the simplest solution is to attenuate the laser pulse before it reaches the photodetector.

ATTENUATION AND FILTERS

The signal may be attenuated with a variety of filters, some of which are suitable but most are not. What characteristics must these filters have in order to be considered suitable? They must withstand the high powers produced by a ruby laser without damage, they must attenuate reproducibly, and, for convenience, their optical densities should be additive when they are used in series. Usually in laser work, one can determine suitability of a component by using it once. If it is not suitable, there will be enough damage done to warrant discarding the component. This test however does not always work. One obvious example of a filter with poor characteristics is a cryptocyanine dye solution; even if

irreversible photochemical damage is not revealed, the high intensity laser light causes the red-absorbing dye to saturate and become transparent. Thus the absorbance after the shot shows the same absorbance associated with low-intensity illumination which was measured prior to the shot. (Here it is assumed that the solution has been prepared so as to avoid decomposition.) Such a filter would cause the photodetector-calorimeter calibration curve (the plot of trace area versus calorimeter energy discussed previously) to deviate positively from a straight line. The first filters used in the attenuation of the photodetector signal behaved in this way and were considered saturable.

Initially the TRG 105B photodetector was chosen as the energy measuring device. The TRG has the capacity to accept internally 2" diameter filters such as those used in photographic work. Tiffen neutral density filters seemed to be suitable. Not only did they fit in the photodetector, but they were also mounted, and they were available in convenient densities to simplify additivity and provide several orders of magnitude variation. The importance of mounting filters must be noted, as the absorbance of two filters would be different if the two filters were spaced rather than if the faces of the two filters were in intimate contact. The reason for this is that when the faces are separated there are four glass to air boundaries at each of which a small fraction of the incident light is lost to reflection. These reflections are included in the manufacturer's assertions about the net

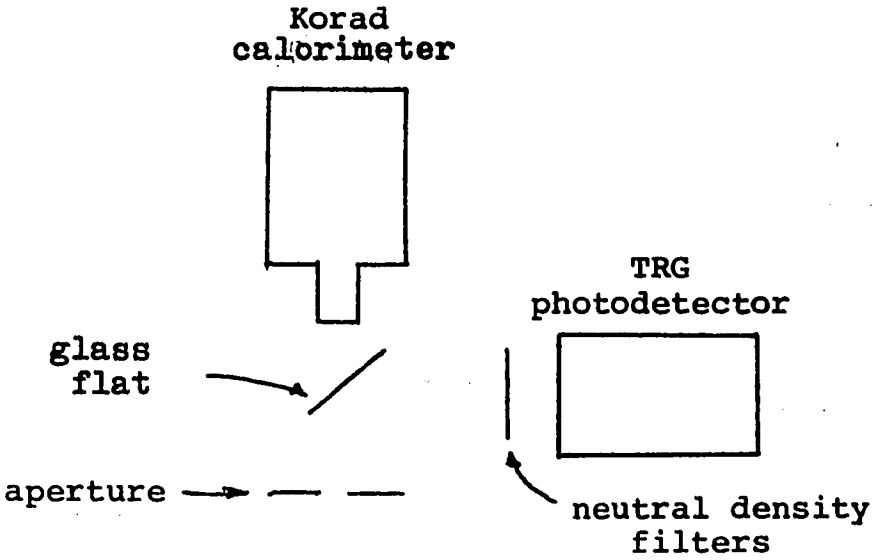

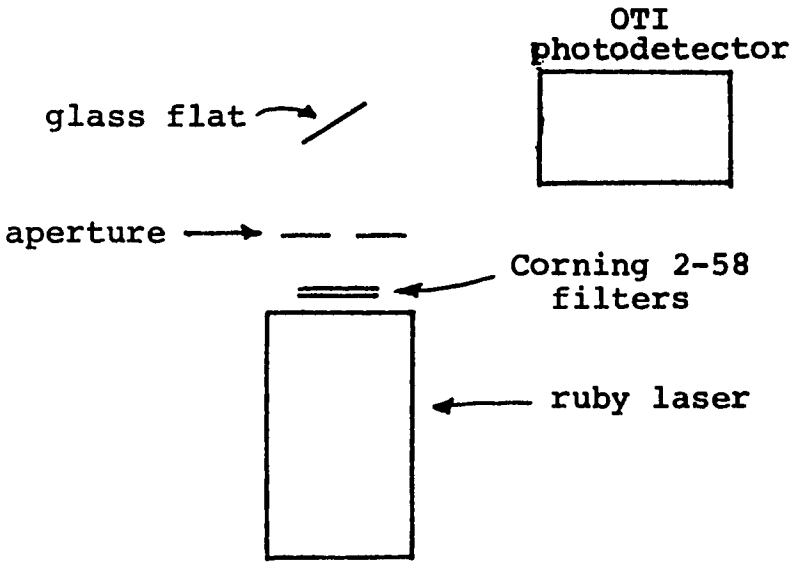

Figure 4

First Arrangement of Apparatus

transmittances of the filter. When two faces of different filters are in contact, there are only two glass to air boundaries and thus less light is lost to reflections. This shows up as a decrease in the "absorbance" of filter pair, from that calculated as the sum of the individual "absorbances." "Absorbance" is equivalent to ln(1/T). Even if one is willing to accept this departure from additivity and place the filters in intimate contact an even worse problem occurs: it is very difficult to eliminate totally all of the air between the two glass surfaces. As filters are changed, from one experiment to the next, different sizes of "air-gaps" would occur, leading to a loss of reproducibility in "absorbance" of the pair of filters.

The data showing saturation of the Tiffen filters are in Table I and are shown graphically in Fig. 5. Other dye filters in which saturation was observed but was not expected were several of the Corning filters which are commonly used in laser work.

Other methods of attenuation were considered and rejected; a few of these are discussed below. Dielectric-coated neutral density filters are produced which can withstand the high powered laser pulses; however, the density of two filters in series is not equal to the sum of the densities of each. The reason for this phenomenon is that the filters work by eliminating light by reflection rather than absorption. Thus, because of multiple reflections between two such filters, the transmittance of two filters in series

is not equal to the product of the transmittances of each. Therefore

$$A_1 + A_2 \neq A_{pair}$$

where A is "absorbance." The magnitude of A_{pair} depends on the distance between the two filters even more sensitively than in the case of the Tiffen filters. For a more detailed explanation the reader may refer to Born and Wolf.[8] Even though this difficulty in using the filters can be overcome, it still must be considered a nuisance and if care is not taken, it can lead to misleading data. A secondary problem with this type of filter is that they are quite expensive.

Another possible method of attenuation would be with the use of diffuse transmitters or diffuse reflectors. One can use the inverse square law to determine transmitted intensities. Although the diffuse transmitter method works well, few laboratories have the necessary space for an optical bench five or more meters long. Even five meters is not sufficient to provide all of the variation needed for several orders of magnitude of attenuation. A combination of one dielectric filter and a sliding diffuse transmitter on a two meter optical bench should work well; however, the alignment is very critical, and one must give a lot of consideration to stray reflections bypassing the diffuse transmitter and directly striking the phototube. Although the entire room was painted flat black, and black felt curtains were placed along optical paths, and all work was done in near total darkness, reproducible results were never obtained with this combina-

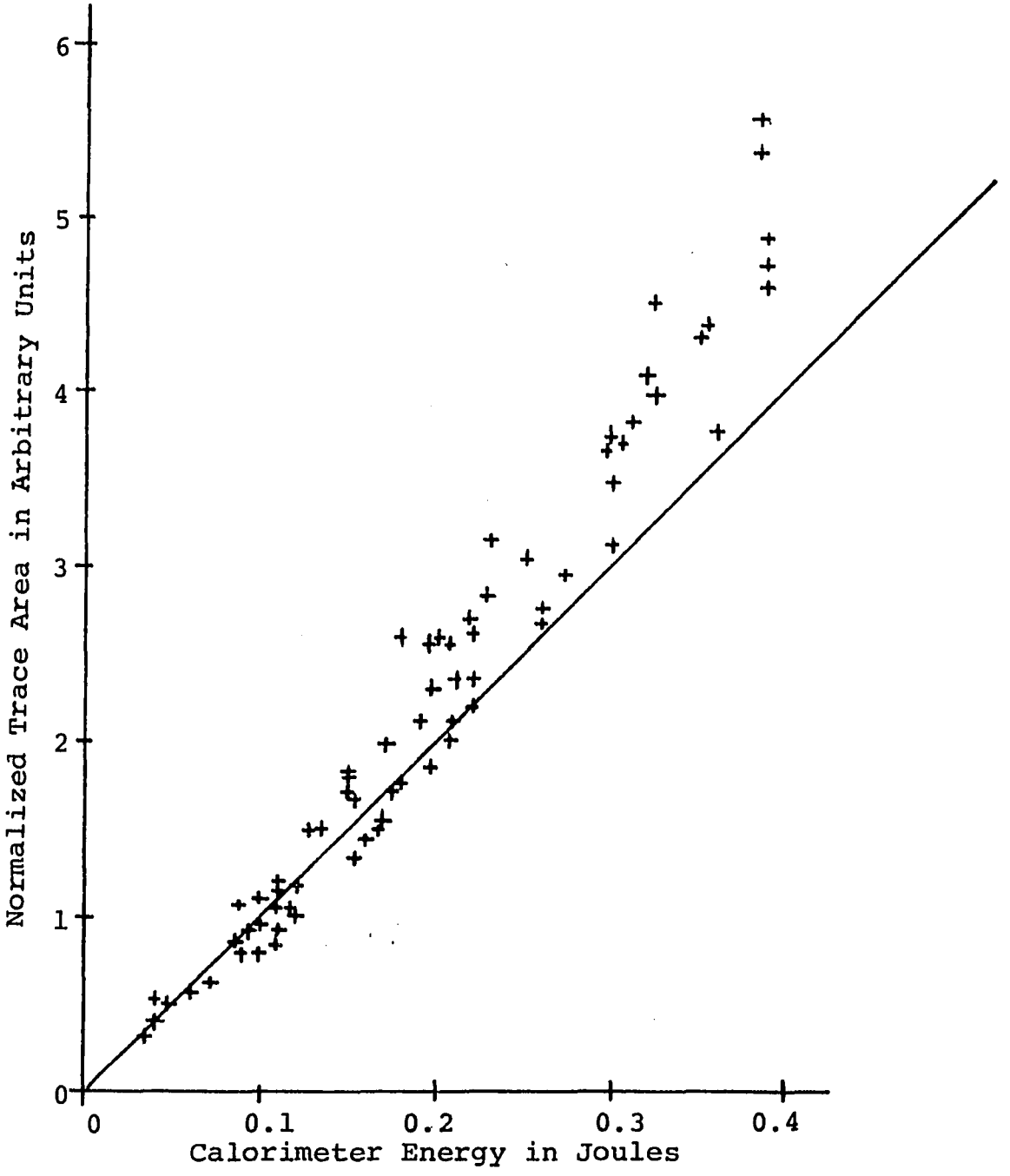

Figure 5

Photodetector Calibration

with Saturable Filters

TABLE I

Photodetector Calibration with Saturable Filters

Laser Shot Number	Normalized Trace Area	Calorimeter Energy in Joules x 10
1178	120 ± 2	1.1 ± 0.1
1181	118 ± 2	1.2 ± 0.2
1182	179 ± 3	1.5 ± 0.1
1183	183 ± 3	1.5 ± 0.2
1184	168 ± 3	1.5 ± 0.2
1185	137 ± 2	1.3 ± 0.1
1186	108 ± 3	0.87 ± 0.07
1187	58 ± 1	0.6 ± 0.1
1189	81 ± 1	0.90 ± 0.09
1191	56 ± 1	0.4 ± 0.1
1192	115 ± 1	1.1 ± 0.1
1194	116 ± 2	1.01 ± 0.07
1195	38 ± 1	0.36 ± 0.06
1197	267 ± 4	2.6 ± 0.1
1202	348 ± 5	3.0 ± 0.1
1205	462 ± 6	3.9 ± 0.2
1206	377 ± 8	3.6 ± 0.1
1207	254 ± 5	2.08 ± 0.08
1209	198 ± 3	1.74 ± 0.08
1210	212 ± 4	2.09 ± 0.05
1211	210 ± 4	1.9 ± 0.1
1212	219 ± 4	2.2 ± 0.1
1213	230 ± 3	1.97 ± 0.05

Laser Shot Number	Normalized Trace Area	Calorimeter Energy in Joules x 10
1214	235 ± 3	2.10 ± 0.05
1215	293 ± 4	2.67 ± 0.09
1216	350 ± 5	3.0 ± 0.1
1217	398 ± 6	3.26 ± 0.04
1219	305 ± 4	2.5 ± 0.2
1221	314 ± 4	3.0 ± 0.1
1222	373 ± 5	3.05 ± 0.04
1223	315 ± 3	2.3 ± 0.2
1228	95 ± 2	1.0 ± 0.2
1230	236 ± 2	2.2 ± 0.1
1231	166 ± 1	1.51 ± 0.09
1232	145 ± 2	1.60 ± 0.09
1233	177 ± 2	1.79 ± 0.05
1234	184 ± 2	1.96 ± 0.05
1235	148 ± 1	1.29 ± 0.05
1236	172 ± 1	1.77 ± 0.03
1237	157 ± 1	1.69 ± 0.08
1238	134 ± 1	1.53 ± 0.09
1239	151 ± 2	1.66 ± 0.03
1240	201 ± 2	2.07 ± 0.03
1241	259 ± 3	1.8 ± 0.2
1242	269 ± 3	2.19 ± 0.08
1243	277 ± 4	2.6 ± 0.1
1244	261 ± 4	2.2 ± 0.1
1245	259 ± 2	2.01 ± 0.09
1248	257 ± 5	1.97 ± 0.09

Laser Shot Number	Normalized Trace Area	Calorimeter Energy in Joules x 10
1251	283 ± 4	2.29 ± 0.08
1252	488 ± 8	3.9 ± 0.1
1257	376 ± 5	3.0 ± 0.2
1258	473 ± 6	3.9 ± 0.1
1259	433 ± 5	3.5 ± 0.1
1260	382 ± 5	3.12 ± 0.08
1261	411 ± 5	3.2 ± 0.1
1262	366 ± 5	2.98 ± 0.05
1263	539 ± 6	3.87 ± 0.05
1264	558 ± 6	3.87 ± 0.08
1265	451 ± 5	3.23 ± 0.05
1266	439 ± 8	3.55 ± 0.08
1270	91 ± 1	1.10 ± 0.03
1271	51 ± 1	0.45 ± 0.05
1272	107 ± 1	1.08 ± 0.05
1274	103 ± 1	1.1 ± 0.1
1275	84 ± 1	0.85 ± 0.08
1276	80 ± 1	0.98 ± 0.05
1277	104 ± 1	1.15 ± 0.05
1278	101 ± 1	1.2 ± 0.1
1279	92 ± 1	0.93 ± 0.05
1280	83 ± 1	1.08 ± 0.09
1284	40 ± 1	0.40 ± 0.05
1285	64 ± 1	0.7 ± 0.1

tion. There was a tremendous amount of scatter in the data which could never be eliminated and presumably was caused by stray reflections. Actually there is often enough dust in the air to scatter sufficient light to produce a signal in the OTI 620 photodetector. Diffuse reflectors are of little value because of alignment difficulties.

Kodak Wratten neutral density filters consist of a colloidal carbon dispersion in gelatin. Such a filter should not and does not saturate. The disadvantage of these filters is that they are losing favor with photographers to the more durable Tiffen neutral density filters. Because of this they are no longer available in a mounted form. Considerable care must be taken in mounting the filters because of the delicate nature of the gelatin. Since it is impossible to get perfect contact between the gelatin and glass flats, it is best to separate them intentionally in order to eliminate wide interference rings. One final plus about these filters (besides the fact that they worked) is that they are by far the least expensive.

The optical alignment used in calibrating the OTI photodetector with the Wratten filters is shown in Fig. 3. The results of that calibration are shown in Table II and Fig. 6. About midway in the course of work a sudden decrease by about a factor of three in photodetector sensitivity was observed. The reason for this change was never found, but a second calibration was required and the results of that calibration are shown in Table III and Fig. 7. The first

calibration was of a quality which was much better than anticipated and has an uncertainty in the slope of less than one percent. The second calibration was performed under more hurried conditions and with fewer data points. The uncertainties were therefore greater but still less than initially anticipated--about three percent. The slopes and corresponding uncertainties were determined using a weighted least squares determination forced to the origin by the methods described by Young.[9]

Theoretically in such an analysis there should be no uncertainties in the independent variables. Application of the least squares method with uncertainties in both coordinates seemed to be more time consuming than its value would warrant. In order to approach the theoretical conditions prescribed, the quantity that seemed to be most precisely measured, the normalized trace area, was plotted along the x-axis even though it seems more natural to use the calorimeter energy as the independent variable. The normalized trace area is corrected for differences in oscilloscope sweep rates and photodetector filter densities.

From the oscilloscope trace it is possible to measure the pulse width and, with the aid of the calibration curves, the energy of the pulse. Also the approximate value of the peak power may be obtained by dividing the pulse energy by the pulse width. For a more accurate peak power determination it is necessary to calculate the ratio of power to pulse height geometrically. This is done by creating an

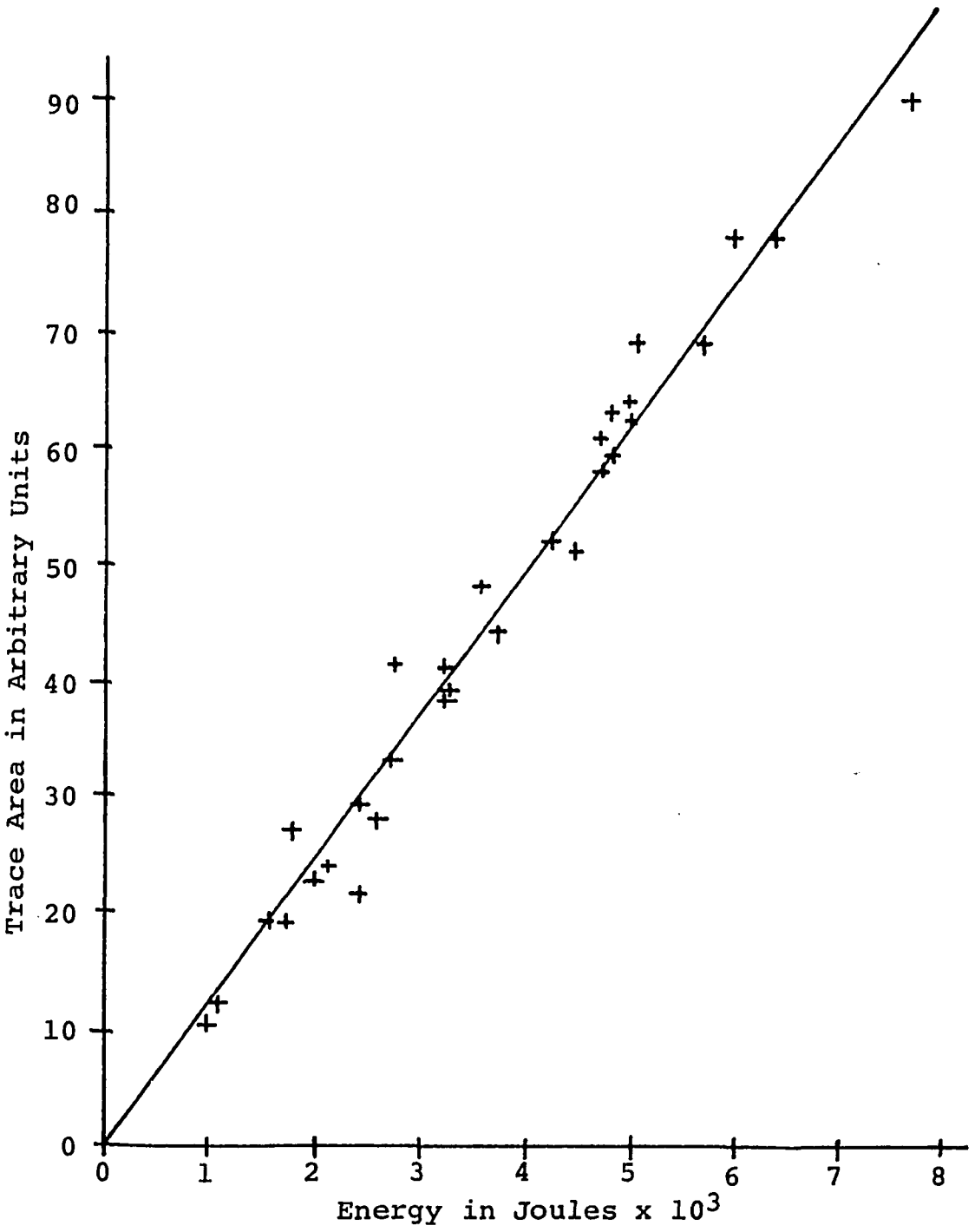

Figure 6

First Calibration of OTI Photodetector

TABLE II

First Calibration of OTI Photodetector

Laser Shot Number	Normalized Trace Area	Incident Energy on Photodetector in Joules x 1000
1693	22.4 ± 0.5	2.0 ± 0.1
1696	41 ± 2	3.2 ± 0.3
1698	27 ± 2	1.8 ± 0.2
1702	41 ± 3	2.7 ± 0.3
1703	38 ± 2	3.2 ± 0.2
1707	29 ± 2	2.4 ± 0.1
1708	24 ± 1	2.1 ± 0.2
1709	28 ± 1	2.6 ± 0.2
1712	12.3 ± 0.7	1.1 ± 0.2
1713	10.5 ± 0.5	1.0 ± 0.2
1714	19.0 ± 0.9	1.7 ± 0.2
1715	19 ± 1	1.6 ± 0.3
1716	21.7 ± 0.8	2.4 ± 0.3
1717	44 ± 4	3.7 ± 0.2
1718	39 ± 3	3.3 ± 0.2
1719	52 ± 3	4.2 ± 0.2
1720	61 ± 2	4.7 ± 0.3
1721	33 ± 2	2.7 ± 0.1
1722	69 ± 2	5.1 ± 0.3
1723	59 ± 2	4.8 ± 0.2
1724	63 ± 2	4.8 ± 0.2
1725	48 ± 2	3.6 ± 0.2
1726	58 ± 2	4.7 ± 0.2

Laser Shot Number	Normalized Trace Area	Incident Energy on Photodetector in Joules x 1000
1727	51 ± 2	4.4 ± 0.2
1729	78 ± 1	6.4 ± 0.3
1730	69 ± 1	5.7 ± 0.3
1731	64 ± 2	5.0 ± 0.2
1732	62 ± 4	5.0 ± 0.2
1733	58 ± 3	4.7 ± 0.2
1737	78 ± 4	6.0 ± 0.3
1738	90 ± 4	7.7 ± 0.4

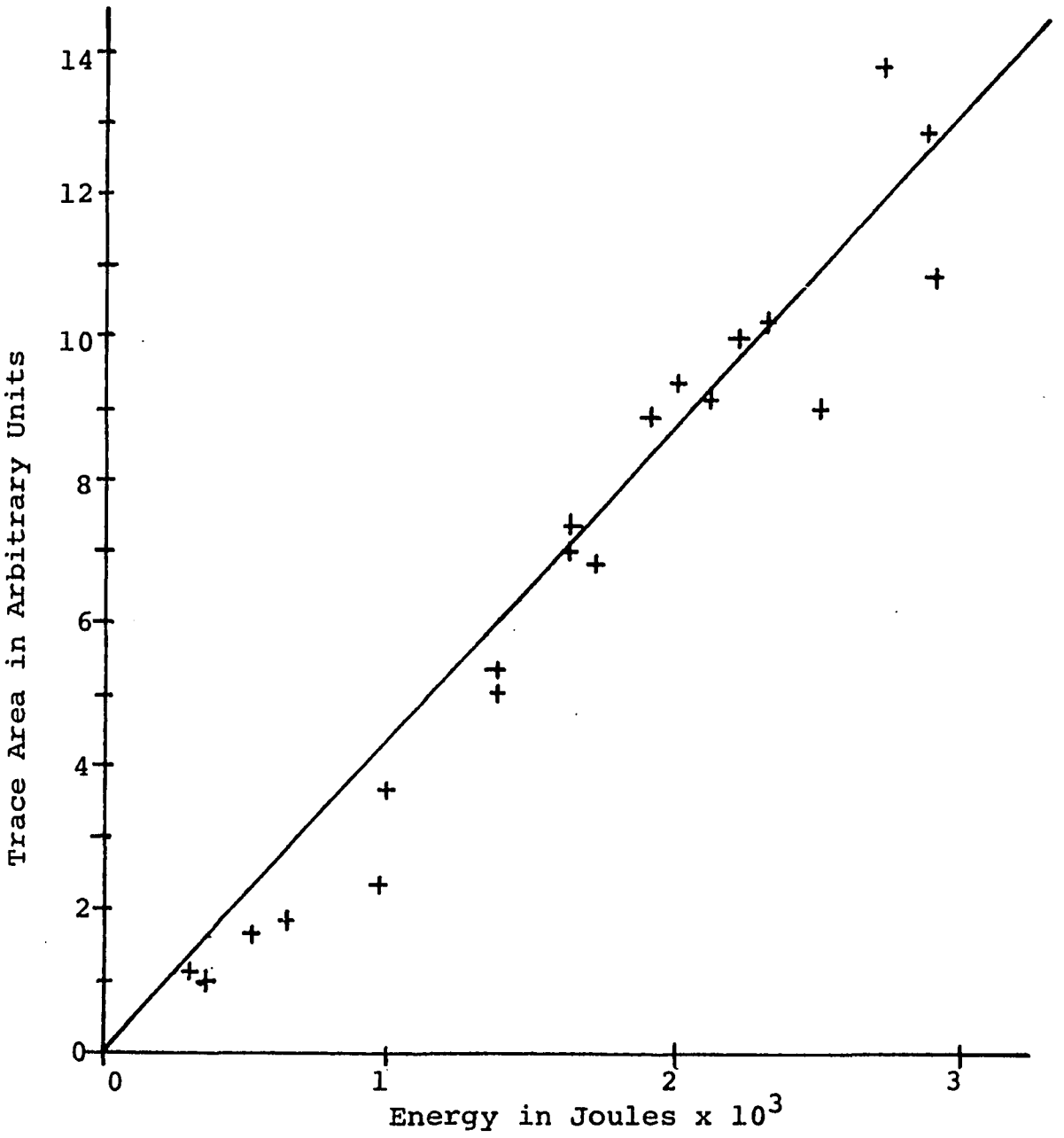

Figure 7

Second Calibration of OTI Photodetector

TABLE III

Second Calibration of OTI Photodetector

Laser Shot Number	Normalized Trace Area	Incident Energy on Photodetector in Joules x 1000
2018	7.0 ± 0.2	1.6 ± 0.1
2019	5.3 ± 0.1	1.30 ± 0.09
2020	6.8 ± 0.3	1.7 ± 0.1
2021	10.8 ± 0.9	2.9 ± 0.1
2025	8.8 ± 0.5	1.9 ± 0.1
2026	10.2 ± 0.4	2.3 ± 0.1
2027	2.3 ± 0.3	0.97 ± 0.09
2028	5.0 ± 0.5	1.35 ± 0.09
2030	3.7 ± 0.2	1.01 ± 0.09
2034	1.58 ± 0.05	0.54 ± 0.06
2035	1.80 ± 0.04	0.66 ± 0.08
2037	1.15 ± 0.04	0.30 ± 0.05
2038	1.03 ± 0.04	0.38 ± 0.05
2039	9.0 ± 0.7	2.5 ± 0.1
2040	7.3 ± 0.6	1.6 ± 0.1
2041	9.1 ± 0.4	2.1 ± 0.1
2042	12.8 ± 0.4	2.9 ± 0.1
2043	10.0 ± 0.5	2.2 ± 0.2
2044	9.3 ± 0.4	2.0 ± 0.2
2045	13.8 ± 0.3	2.7 ± 0.2

imaginary rectangular pulse of height V and width t; see Fig. 8. Using the pulse area Vt in units of V·ns, the pulse width t in ns, and the previously determined pulse energy-to-pulse area ratio, the power-to-pulse height ratio may be determined. This was found to be 119 $\pm$ 2 W/V for the first calibration and 320 $\pm$ 10 W/V for the second calibration.

With the photodetector quite precisely, and hopefully quite accurately, calibrated, it is possible to make some accurate and precise measurements with a ruby laser. One of these will be discussed in the next chapter.

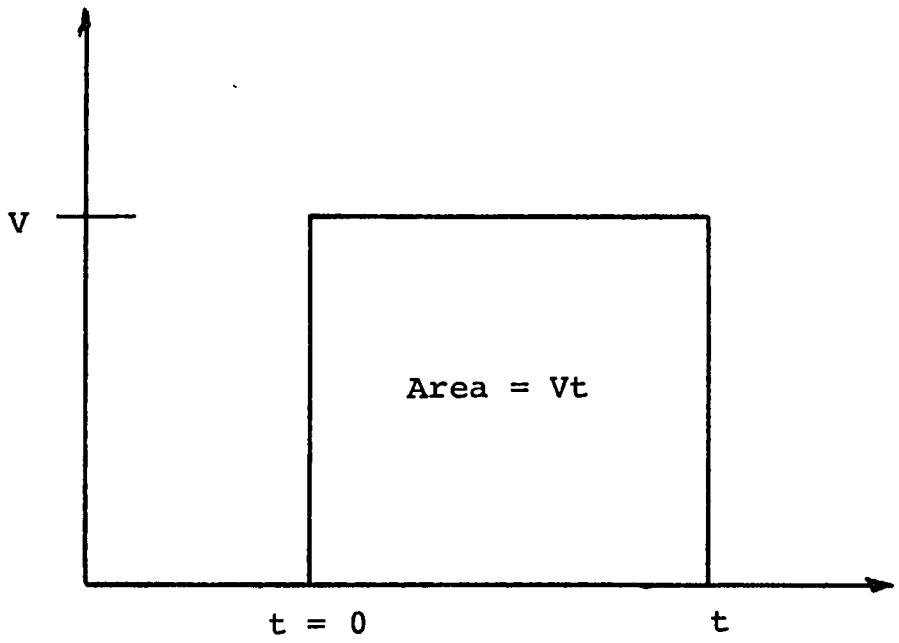

Figure 8

Rectangular Pulse

PART I - CHAPTER II

A PRECISION MEASUREMENT OF LASER INDUCED RECIPROCITY FAILURE

INTRODUCTION

In Chapter I various instruments were used to monitor laser pulses from the ruby laser. These were calibrated so that the total energy, pulse width, and peak power could be measured for each single laser shot. With these quantities it is possible to use the ruby laser as a precise quantitative tool, whereas in the past it has been used primarily in qualitative spectroscopy.

Spectrograms were once prepared by a two-step process. First, the light emitted or transmitted by a sample was dispersed by grating or a prism and then allowed to fall upon a photographic plate or film in a spectrograph. The film was then developed and scanned by a photoelectric densitometer to produce a quantitative record of the relative intensities of the spectral lines.

In modern spectroscopy, the spectrograph and the densitometer are combined into a single device called the photoelectric spectrophotometer. Where the film or plate holder would be found in a spectrograph, one finds instead an exit slit in this instrument. A scanning motor then turns a dispersing element so that the rays of light having different wavelengths are fed sequentially into the exit slit. Finally, light which passes through the exit slit is detected by a

photoelectric element. The combined instrument has fewer parts and therefore costs less to purchase and maintain than the two instruments it replaced. An even more important advantage of the spectrophotometer is the increased convenience in use, since the time and trouble required to purchase, store, expose and develop the photographic emulsions for the spectrograph/densitometer is eliminated. Because of its disadvantages, photographic spectroscopy nearly became extinct when spectrophotometers became widely available.

However, there is one recent scientific development which seems destined to restore the spectrograph/densitometer combination to a position of importance in spectroscopy: the invention of the laser. As was stated in Chapter I, lasers are available which produce a continuous beam of light, and when these are used as excitation sources for spectrographic studies, the modern spectrophotometer can be used to record the spectra. It was also noted, however, that many interesting non-linear optical phenomena can be observed only if the excitation source is a pulsed laser, because only pulsed lasers can produce sufficient power to produce these non-linearities in the sample. Pulsed lasers produce such brief bursts of light that no spectrophotometer can scan rapidly enough to record the spectra excited by them. This is not a mere technological limitation to be overcome by clever engineering, but a fundamental physical limitation, as can be seen by the following argument. Some of the light emitted or transmitted by a sample is as brief in

duration as the laser pulse used to excite the sample, so that the entire spectrum must be recorded in a time which is short in comparison with the duration of this pulse. A ruby or neodymium laser pumped by a xenon flash lamp usually produces pulses lasting a few microseconds, and special techniques enable a further reduction in pulse duration by three or even six orders of magnitude. The tangential velocity which a prism or grating would have to achieve (in order to move each spectral line over the exit slit before the pulse terminated) greatly exceeds the speed of light, which is impossible. Therefore, spectrophotometers are not satisfactory instruments for recording spectra of materials excited by pulsed lasers.

This problem can be overcome by returning to the spectrograph/densitometer combination. The photographic emulsion in the spectrograph is irradiated simultaneously by all rays coming from the dispersing element, and the resulting spectrogram can be subsequently analyzed at leisure by the densitometer. It makes no difference whether or not the pulse is long or short, since the dispersing element instantaneously separates the rays of different wavelength and directs them to different portions of the emulsion. To put it another way, the spectrograph provides a practically infinite number of parallel channels for the simultaneous recording of information, while the spectrophotometer has only one channel through which the information must pass serially. The former instrument, in combination with the densitometer, is therefore suitable for the recording of spectra of samples excited by pulsed

lasers, and the latter instrument is not suitable. In Chapter I, a cautionary note was sounded: before giving way to unrestrained rejoicing about the simplicity of this solution to the pulsed-laser spectra problem prudence dictates that consideration as to whether or not the special characteristics of laser beams might cause the photochemical behavior of photographic emulsions to differ from that encountered when exposures are made with conventional light sources. First, the very great intensity of the beams will not cause any problems. This is because linear, accurate and reproducible attenuators for these beams are available as discussed in Chapter I, and can be placed between the sample and the entrance slit of the spectrograph. The light can thereby be attenuated to a level at which the degree of blackening of the emulsion is accurately proportional to the number of photons striking the film or plate. Second, the coherence of the beam will not cause any problems because various methods are available for scrambling the phases of the waves which otherwise might produce interference effects within the emulsion. The simplest of these methods consists of separating the laser from the emulsion by several coherence-lengths; another method consists of using a diffuse filter between the laser and the emulsion.

The only remaining potential source of difficulty is the very brief duration of the pulses, and indeed this is likely to cause problems for which there are no simple remedies. In elementary photochemical processes, the mass of the photoproduct is proportional to the exposure, E, defined as

intensity of the light source, I, times the exposure time, t. This fact, first noted in 1862 by Bunsen and Roscoe,[10] is called the Reciprocity Law because of the inverse relationship it establishes between the I and t associated with a given amount of reaction. The physical basis for the Reciprocity Law is very simple; each photon striking the sample is assumed to have an equal probability (quantum efficiency) of producing a photochemical reaction in one molecule, and the total number of incident photons is proportional to the exposure.

Since the opacity of a developed emulsion is indeed proportional to the mass of the silver reduced in the overall photographic process, it might be hoped that the Reciprocity Law would apply to the associated photochemistry. Indeed, over a wide range of experimental conditions, the amount of blackening produced in photographic emulsions by a given number of photons is independent of exposure time. Unfortunately, for very long or very short exposure times, the Reciprocity Law fails.

Since pulsed lasers are characterized by extremely short exposure times, one may then expect severe departures from the Reciprocity Law (reciprocity failure) when using them to expose photographic emulsions. The reason for reciprocity failure cannot be understood without a detailed examination of the kinetics and mechanism of the process by means of which photons produce latent images in photographic emulsions. A summary of what is known about this subject is

presented in the appendix.

Before reading the appendix, one should know that it is customary to call reciprocity failure at short exposure times "high-intensity" reciprocity failure. In the present context, this nomenclature is somewhat misleading since it suggests that the intensity of a high-powered laser beam cannot be quantitatively reduced before it is used to expose photographic emulsions. As has been previously noted, linear and reproducible attenuators for pulsed lasers can be made. Nevertheless, enough light must be admitted to blacken the emulsion by a detectable amount. For very short exposure times this may require a photon flux which is large in relation to the rates of the photochemical processes associated with the formation of the latent image, even if the light intensity reaching the film or plate is very much less than that which left the laser. Therefore, when reading the appendix, one should probably interpret the phrase "high-intensity reciprocity failure" as "reciprocity failure due to brief exposure-times."

The objective of this chapter is to use the results of Chapter I to measure the degree of reciprocity failure in a photographic emulsion exposed to very brief pulses of light produced by a laser. The significance of this study can be easily seen from the material presented in the preceding paragraphs. No quantitative spectroscopic measurements can be made using pulsed lasers or a light source until the data on reciprocity failure in the films used are available. The

information provided in this chapter will enable persons studying laser-induced non-linear optical phenomena such as frequency doubling and stimulated Raman scattering to correct photographic records of their experiment for the reciprocity failure. The corrected results may then be used with confidence in calculating accurate threshold intensities and gain coefficients for these effects. Finally, these experimental values can be compared with those computed from the various theoretical models of non-linear optical behavior, in order to provide a quantitative test of the latter.

Hercher and Ruff[11] found severe high-intensity reciprocity failure in Kodak 649-F spectroscopic plates exposed to light from a pulsed ruby laser. The amount of light energy required to produce a given amount of film blackening increased by an order of magnitude when the exposure time was decreased from 60 seconds to 250 microseconds. They noted the effects of post-exposure of the emulsion, development time, and development temperature upon the reciprocity failure, and found image halation at high intensities. They claim an accuracy of 5% for their measurements of exposure and 10% for their measurements of optical density.

The 60 s exposures were produced by means of a tungsten lamp and 694 nm-transmitting filters, the 250 μs exposures by a train of 3 to 4 μs pulses from their laser, and the 15 ns exposures by single Q-switched pulses from the same laser. Whether or not an exposure produced by means of 75 pulses of more or less constant intensity and of 3.5 μs

duration is equivalent to one produced by means of a single exposure of the same intensity lasting 260 μs depends upon the grain size in the emulsion, the light intensity, and the (dark) time between the pulses.[12] There is no way to tell from the information provided in the paper whether or not the authors took the necessary precautions to ensure that, in their particular case, the two exposures are indeed equivalent as they have assumed.

The graphs of the experimental results provided by the authors suggest that their estimates of random error are quite conservative. The evident care exercised by them in controlling the conditions of development of the plates inspires confidence in their data for Kodak 649-F plates exposed to 694 nm light, at least for 60 seconds and 15 ns exposure times.

Further, it is evident from their work that investigations should be made for other exposure times, for other photographic emulsions, and using other lasers, if quantitative information is to be obtained from photographic spectrograms produced under such conditions.

A number of different pulsed lasers are currently available, and each of these produces light at a different wavelength. The two most important ones are the neodymium laser (λ = 1.06 μm) and the ruby laser (λ = 694 nm). Since a ruby laser was readily available, we chose it as the light source for our experiments. The spectrograph we plan to employ in future work requires 35 mm film. A convenient

choice is Kodak High Speed Infrared (HIE) which has a good sensitivity for light with wavelengths in the region of 694 nm. Therefore, our first task was to measure the amount of blackening of HIE film produced by a given constant number of ruby-laser-produced 694 nm photons for a number of different exposure times.

THE IDEAL EXPERIMENT

In order to get a full picture of reciprocity failure it would be desirable to obtain data over several orders of magnitude in exposure time. Since a pulsed ruby laser can be used as a light source over a very small range of exposure times, other light sources are needed to obtain the longer pulses. It was hoped that a conventional light source (continuous white light, tungsten filament with appropriate filters) and a camera shutter could be used to produce the exposures from 10^{2} to 10^{-3} seconds. However, in practice, because so much of the light intensity was lost in passing through a 694 nm narrow band pass filter, the 10^{-1} to 10^{-3} second exposures could not be obtained with this light source.

For the exposure times of 10^{-3} to 10^{-4} seconds a pulsed source (a xenon flash lamp and filter) could be used. However, with such a light source there was not sufficient instrumentation available. The photodetectors described in Chapter I were far too insensitive to measure the intensity of this light source. Finally it was hoped that the laser itself would provide pulses of 10^{-4} to 10^{-8} seconds. This turned out to be impossible with the available laser and photodetectors.

When trying to obtain pulses longer than 10^{-7} seconds, it is nearly impossible to eliminate multiple pulses and again the available calibrated photodetectors were not sensitive enough to detect the signals of the low power produced from the longer pulses.

Because of these difficulties it was decided to gather data only in the readily accessible laser exposure time range of 10^{-7} to 10^{-8} seconds. Along with this the data were gathered for a one second exposure simply for comparison and to demonstrate the effect of reciprocity failure.

EXPERIMENTAL

The basic procedure involved in obtaining reciprocity curves is as follows: (1) expose the film with various intensities at a given exposure time and then (2) measure the amount of blackening produced in the film by the exposure. The results of this data may then be used to plot the H & D curve (see appendix), which gives the relationship between exposure and film density at a particular exposure time. Upon obtaining several of these curves for different exposure times, a set of reciprocity curves may be determined by plotting log (I·t) vs. log I for a given film density (see appendix).

As in the procedure of calibrating the photodetector, many optical arrangements were tried. The one finally used for the laser exposures is shown in Fig. 4, Chapter I. Each component except for the camera was discussed in detail in Chapter I and will not be covered here.

The 35 mm Argus camera actually served as nothing but

a light-tight film holder. All of the lenses were removed and a large diameter shutter replaced the smaller original shutter. The original shutter had an aperture with a maximum opening of only about 1.5 cm. It was soon learned that since the laser frequently fires off axis, a varying portion of each laser shot was stopped by the shutter. The larger shutter had a 2.6 cm opening, which was large enough to "see" the same cross-sectional beam area as the calibrated photodetector.

A diffuse filter was attached to the camera 10.0 cm in front of the film plane. It was made of a piece of laminated opal glass of a kind frequently used in the diffusing type photographic enlargers. The opal glass layer is about 0.5 mm thick on transparent glass. To improve further the diffusing qualities, the opal side of the glass was hand ground with 400 and then 1000 grit carborundum powder. The resulting diffuse filter was very close to a perfect diffuser in that it obeyed Lambert's inverse square law to better than 1%. This was measured with a Spectra Physics helium-neon laser model 133 (serial no. 1390, 13 mW output at 632.8 nm) and the OTI photodetector. The low power signal produced by the laser light striking the photodetector was monitored by the Keithley microvoltmeter (see Fig. 9). The distance, r, between the diffuse filter and the photodetector was varied; and a plot of voltage (proportional to intensity) versus $1/r^2$ was found to be almost perfectly linear. The diffuser served three purposes: (1) it reduced the intensity of the laser pulses to a convenient amount, (2) it produced a

smooth light distribution which nearly varied in intensity with the cosine of the angle from the axis, and (3) it eliminated any possibility of interference effects in the film emulsion. Exposures without this filter produced solarization and even blackening in adjacent frames on the film. With such high intensities an extremely large amount of light is scattered by the grains in the film emulsion. The film then acts as a light pipe, exposing undesired regions. Reducing the light intensity with non-diffuse filters is not satisfactory because of the uneven distribution of the light produced by the laser. The filter was placed at a distance from the film plane so that there should be less than a 3% variation in light intensity over the entire area of the standard sized 35 mm frame.

Different exposures were obtained by varying the neutral density filters between the laser and the film. The exposure time was held constant by not varying the Q-switch concentration. Before firing the laser, all room lights were turned off, then the shutter was opened using a remote squeeze bulb. After the laser was fired, the pressure was then released, closing the shutter.

A photographic emulsion is capable of good quantitative results; however, great care must be taken to assure that the emulsion has a constant sensitivity. Variations in storage, time between exposure and development, development times, plus the concentration, temperature, agitation, and freshness of the developer solution can have considerable

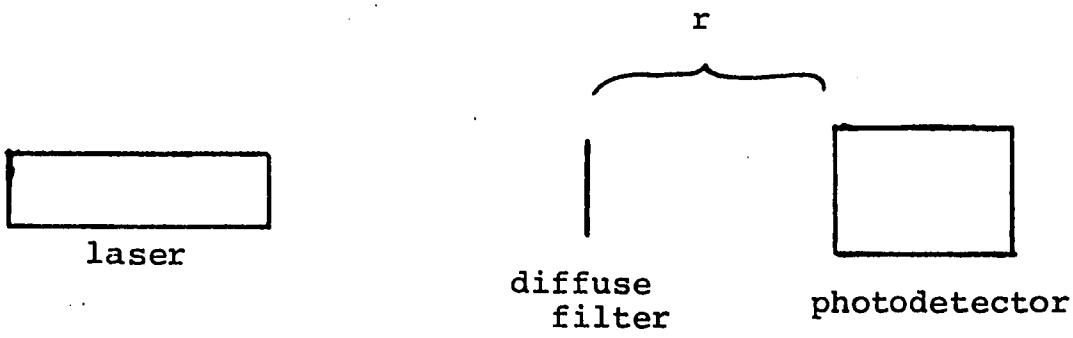

Figure 9

Lambert's Law Apparatus

effect on the relationship between film darkening and exposure. In order to study film darkening versus exposure, i.e., light intensity multiplied by the time, all of these variables must be held as constant as possible. Infrared film is particularly susceptible to heat, thus great care was taken to minimize fogging. Long term (on the order of months) storage of the film was in a freezer at around 0°F. Bulk Kodak High Speed Infrared Film 2481 HIE 421 all from the same emulsion batch (#2481-32-6) was used. Approximately one meter lengths were rolled into 35 mm casettes as needed. After exposure, the film was stored at 20°F to minimize recombination effects, and also developed within 24 hours. The developer (Kodak D-76) was also refrigerated in order to maintain quality. The contents of each can were well mixed and separated into 210 ± 1 gram quantities. This was added to approximately 1000 ml of distilled water at 52°C with continuous stirring until dissolved. Then cool distilled water was added to make 2000 ± 5 ml at 20.0° ± 0.2°C. (Water was added to almost 2000 ml and then the flask was cooled in ice water to 20°C then brought to exactly 2000 ml).

The developer temperature could be held to 20.0° ± 0.3°C through the development time of 11 minutes ± 10 seconds without elaborate cooling equipment as long as the room was between 66° and 69°F. No film was developed unless room temperature was in this range. A constant agitation was maintained during all but the first and last ten seconds of the development time with a motor driven piston (see Fig. 10).

The total vertical movement was 2" at the rate of one complete stroke per second. Two rolls of film could be developed at once in the two reels attached to the piston. The developer solution was always used within a couple of hours after mixing and no more than four rolls of film were developed per batch.

After development, the film was immediately immersed in a stop bath consisting of a 1.3% solution of acetic acid with constant hand agitation for 25 ± 5 seconds. The film was then fixed with Kodak Rapid Fixer for three minutes, agitating for 10 seconds every 1/2 minute. It was then washed for 1 - 5 minutes, rinsed in Perma-Wash for 1 - 2 minutes and washed again for 1 - 2 minutes. After soaking in Kodak Photo-Flo for 30 seconds, the film was squeegeed and hung to dry.

After drying, the darkening of each exposed frame of film was measured using a modified Hughes-Nauman Densitometer[13] and a Cary 14 spectrophotometer (see Fig. 11). The densitometer intercepts the sample light beam from the spectrophotometer and passes it through the film and then directs it back to the photodetector in the spectrophotometer. The densitometer is semispecular, this particular one having a collection angle of about 45°. Film densities are usually reported in terms of diffuse density[14] because of better standardization. Diffuse densities are lower than semispecular and specular densities, the amount lower depending on grain size and density. A diffuse densitometer collects all of the scattered light that passes through the film, while a specular one collects light over a small angle. Semispecular has a collection

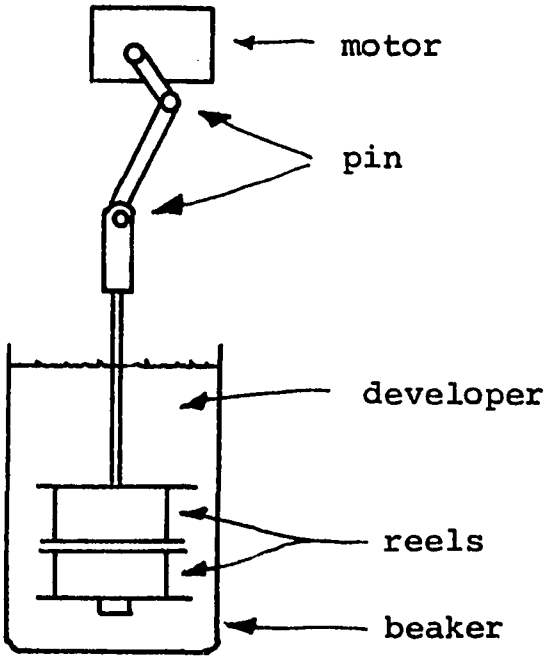

Figure 10

Continuous Agitation Developer

angle between the two. For a moderately coarse grain size such as Kodak High Speed Infrared Film, 24° semispecular densities are about 50% greater than diffuse densities.[15]

Because the 50% figure is only an estimate, the data reported in this dissertation cannot be reported in standard form. However, since the relation between the log of the exposure and film density is a linear one for a wide range of film densities, other data would differ only by a multiplicative constant (or additive constant in terms of log E).

Only two exposure times using the laser were used. It was hoped that the two times could differ by about an order of magnitude. However, the longest single pulse widths possible with this particular ruby laser is about 80 nanoseconds. (Longer pulse widths can be produced but not singly.) The maximum optical density of the dye (at 706 nm) required to produce 80 ns pulses is only 0.1. Lower optical densities than this would not inhibit multiple pulsing. For the shorter times, pulses of about 20 ns could be produced practically. Somewhat shorter pulses could have been produced but only by using extremely high pump powers. High pump powers are required for higher Q-switch concentrations which in turn produce shorter pulses. Since pumping to very high powers is hard on the optical and electrical components of the laser, the short exposure times were obtained at 20 ns.

The total energy striking the film is proportional to the area of the pulse recorded on the oscilloscope. The constant of proportionality is determined from the photodetector

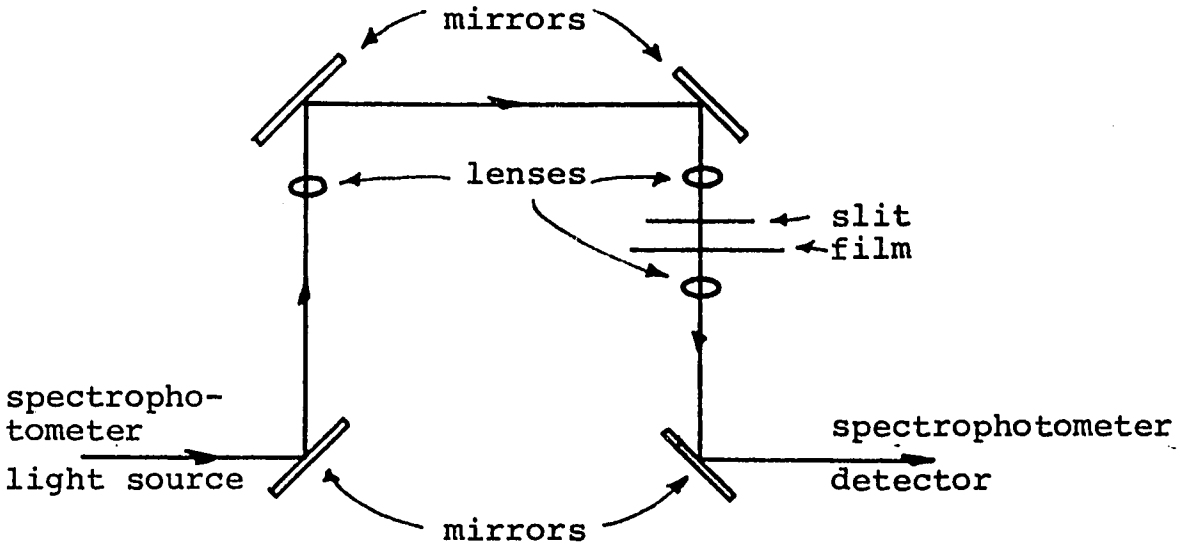

Figure 11

Hughes-Nauman Densitometer Schematic

calibration obtained in Chapter I, the neutral density filters in front of the photodetector, the partial transmitting reflector beamsplitter, the neutral density filters in front of the camera, and the light scattering losses in the diffuse filter attached to the camera.

A quantitative measurement of that loss due to the laser beam passing through the diffuse filter had to be performed. The optical arrangement used is shown in Fig. 12, where H is the Spectra Physics helium-neon laser, L_1 and L_2 are lenses to make the beam less divergent, C is the camera with the diffuse filter attached, and P is the OTI photodetector monitored by the Keithley microvoltmeter. When the light strikes the diffuser the transmitted portion is scattered hemispherically, with the intensity at any given point being proportional to $1/r^2 \cos \theta$ where r is the radial distance from the filter to the point and θ is the angle between the radial line and the normal line to the filter (Fig. 13). Note that the "intensity" has units of energy per length squared; or, in measuring the intensity at a point, obviously the total energy depends on the size of the aperture through which the energy must pass. Therefore an aperture, with a fixed area, was placed in the film plane of the camera. The ratio of the Keithley reading (microvolts), with the camera in place, divided by the area of the aperture, gives the loss factor for the diffuse filter. That factor has units of length^{-2}. The assumption has been made here that the loss factor at 694.3 nm is equal to that

at 623.8 nm, the wavelength of a helium-neon laser. The data and calculations for this loss factor are shown in Table IV.

Now with all the necessary data it is possible to determine the light intensity and duration of each pulse. The product of these two quantities is the total exposure, E. A plot of film density vs. log E, should produce the H & D curve. See Tables V and VI for the data from the 20 and 80 nanosecond exposure groups. Plots of the data may be seen in Figs. 14 and 15.

The one-second exposures were obtained by using a 1000 watt slide projector with appropriate lenses, apertures, and filter to make it somewhat similar, in beam shape at least, to a laser. The apparatus used in this section of the experiment is shown schematically in Fig. 16. In the figure S is the slide projector; A is a 3/8" diameter aperture; F_1 is a 694 nm narrow band pass filter; B is an OTI 20% T dielectric reflector; C is the camera with the diffuse filter; F_2 is a number of Tiffen neutral density filters; P is the OTI photodetector monitored by the Keithley microvoltmeter and a recorder; and K is a 1300 watt constant voltage power supply placed between the slide projector and the A. C. power line. The C. V. power supply helped to minimize fluctuations in light intensity due to voltage changes in the line. Exposures were made with the beam-splitter removed because of the low light intensity actually getting to the camera. Readings of light intensity were taken immediately before and after each exposure.

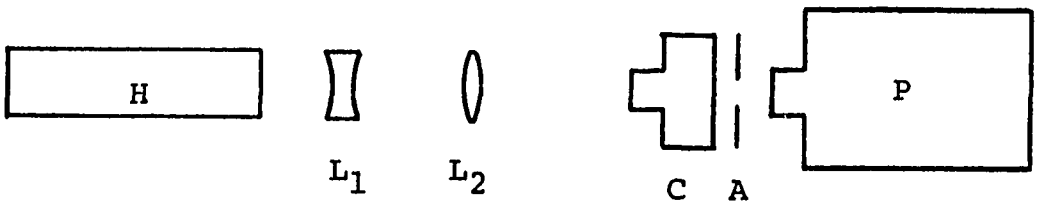

Figure 12

Apparatus for Measuring Camera Loss Factor

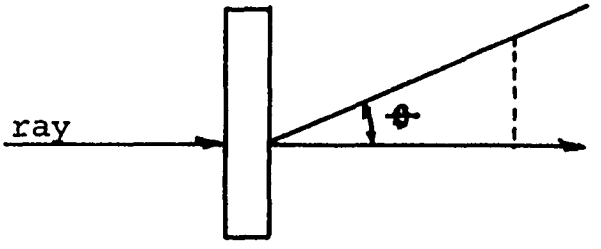

Figure 13

Diffuse Filter

TABLE IV

Camera Loss Factor Data

Aperture diameter = 1.050 ± 0.003 cm

Aperture area, A = 0.866 ± 0.005 cm^2

Detected energy with camera, B = 0.0372 ± 0.0002 mW

Detected energy without camera, C = 30.0 ± 0.1 mW

Camera loss factor, F = $(1.43 \pm 0.01) \times 10^{-3}$ cm^{-2}

$$F = \frac{B}{C} \times \frac{1}{A}$$

TABLE V

Nineteen Nanosecond Exposure Data

Laser Shot Number	Log Exposure	Film Density
1739	-2.79 ± 0.05	1.14 ± 0.02
1740	-2.90 ± 0.05	1.00 ± 0.02
1741	-2.87 ± 0.05	1.02 ± 0.02
1742	-2.85 ± 0.05	1.08 ± 0.02
1743	-2.84 ± 0.05	1.08 ± 0.02
1744	-2.83 ± 0.04	1.04 ± 0.02
1746	-3.77 ± 0.05	0.15 ± 0.01
1747	-3.68 ± 0.04	0.22 ± 0.01
1748	-3.68 ± 0.04	0.20 ± 0.01
1749	-3.66 ± 0.04	0.20 ± 0.01
1750	-3.67 ± 0.05	0.23 ± 0.01
1751	-3.66 ± 0.05	0.24 ± 0.01
1769	-2.35 ± 0.04	1.42 ± 0.02
1770	-2.54 ± 0.06	1.28 ± 0.02
1772	-2.34 ± 0.05	1.38 ± 0.02
1773	-2.29 ± 0.04	1.45 ± 0.02
1774	-2.50 ± 0.06	1.34 ± 0.02
1775	-2.64 ± 0.04	1.18 ± 0.02
1776	-2.90 ± 0.06	0.94 ± 0.01
1777	-2.86 ± 0.07	0.96 ± 0.01
1778	-2.76 ± 0.04	1.14 ± 0.02
1779	-2.60 ± 0.06	1.24 ± 0.02

Laser Shot Number	Log Exposure	Film Density
1780	-2.54 ± 0.04	1.26 ± 0.02
1781	-2.60 ± 0.05	1.22 ± 0.02
1782	-2.51 ± 0.04	1.28 ± 0.02
1783	-3.51 ± 0.05	0.34 ± 0.01
1784	-3.50 ± 0.06	0.34 ± 0.01
1785	-3.38 ± 0.05	0.44 ± 0.01
1786	-3.35 ± 0.05	0.49 ± 0.01
1787	-3.52 ± 0.05	0.33 ± 0.01
1788	-3.55 ± 0.05	0.32 ± 0.01
1789	-3.44 ± 0.05	0.42 ± 0.01
1790	-3.41 ± 0.05	0.48 ± 0.01

The following data is on the non-linear portion of the H & D curve:

1752	-4.06 ± 0.06	0.044 ± 0.005
1753	-4.10 ± 0.06	0.044 ± 0.005
1754	-3.88 ± 0.05	0.128 ± 0.005
1755	-4.01 ± 0.06	0.065 ± 0.005
1757	-4.02 ± 0.06	0.070 ± 0.005
1758	-3.96 ± 0.05	0.094 ± 0.005

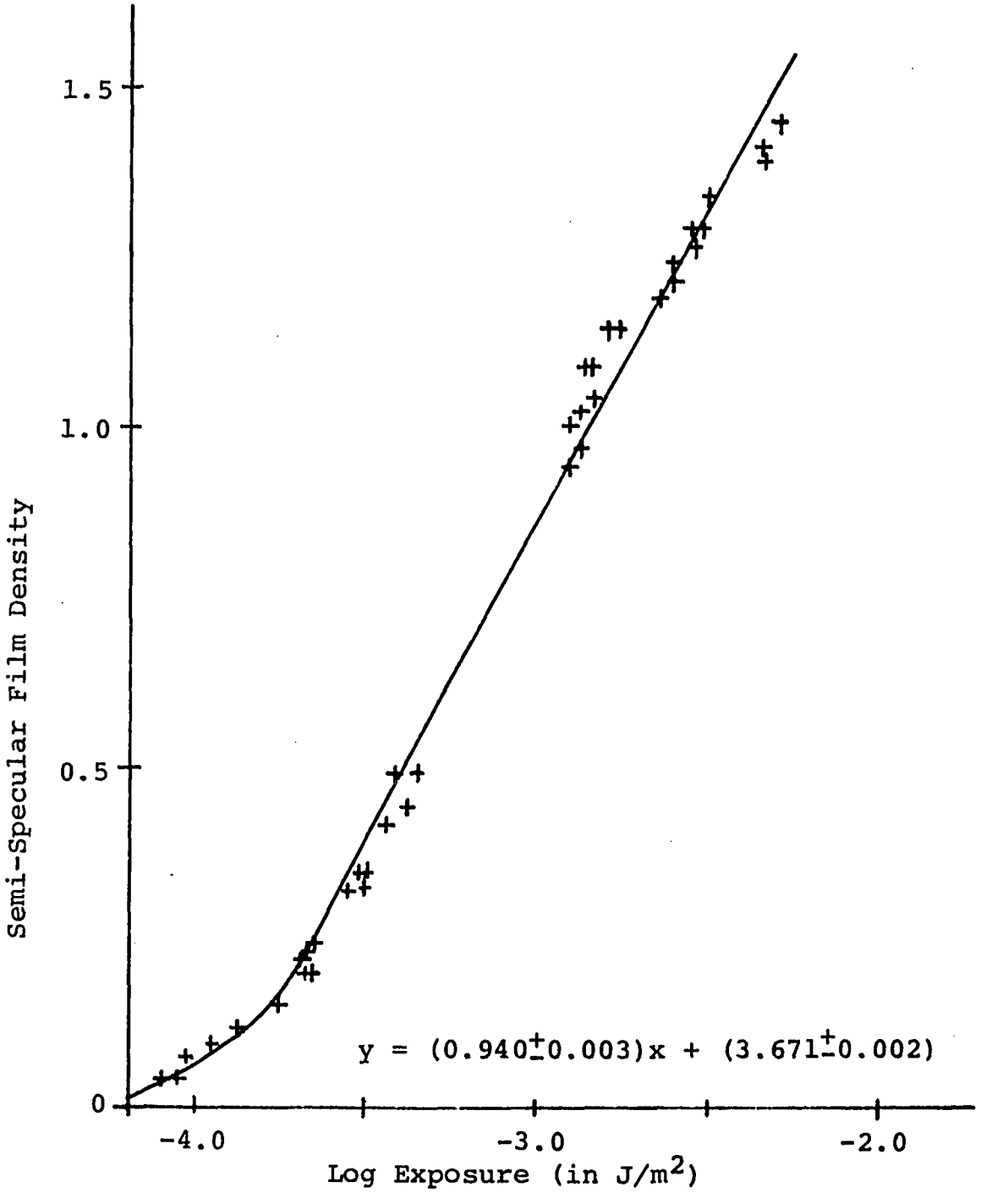

Figure 14

Nineteen Nanosecond Characteristic Curve

TABLE VI

Seventy-five Nanosecond Exposure Data

Laser Shot Number	Log Exposure	Film Density
2247	-2.10 ± 0.06	1.62 ± 0.02
2250	-1.95 ± 0.06	1.66 ± 0.02
2252	-2.47 ± 0.06	1.30 ± 0.02
2262	-2.65 ± 0.08	1.17 ± 0.02
2263	-3.23 ± 0.09	0.60 ± 0.01
2280	-3.18 ± 0.06	0.58 ± 0.01
2283	-3.77 ± 0.05	0.44 ± 0.01
2288	-2.78 ± 0.05	1.32 ± 0.02
2290	-2.79 ± 0.06	1.11 ± 0.02
2292	-3.13 ± 0.05	0.98 ± 0.02
2307	-3.34 ± 0.05	0.42 ± 0.01
2311	-3.08 ± 0.05	0.58 ± 0.01
2313	-3.12 ± 0.06	0.56 ± 0.01
2314	-2.92 ± 0.07	0.70 ± 0.01
2317	-2.75 ± 0.06	0.84 ± 0.01
2318	-2.48 ± 0.06	1.12 ± 0.02
2320	-2.75 ± 0.05	0.87 ± 0.01
2321	-3.34 ± 0.06	0.33 ± 0.01
2324	-2.46 ± 0.06	1.11 ± 0.02
2326	-3.05 ± 0.06	0.76 ± 0.01

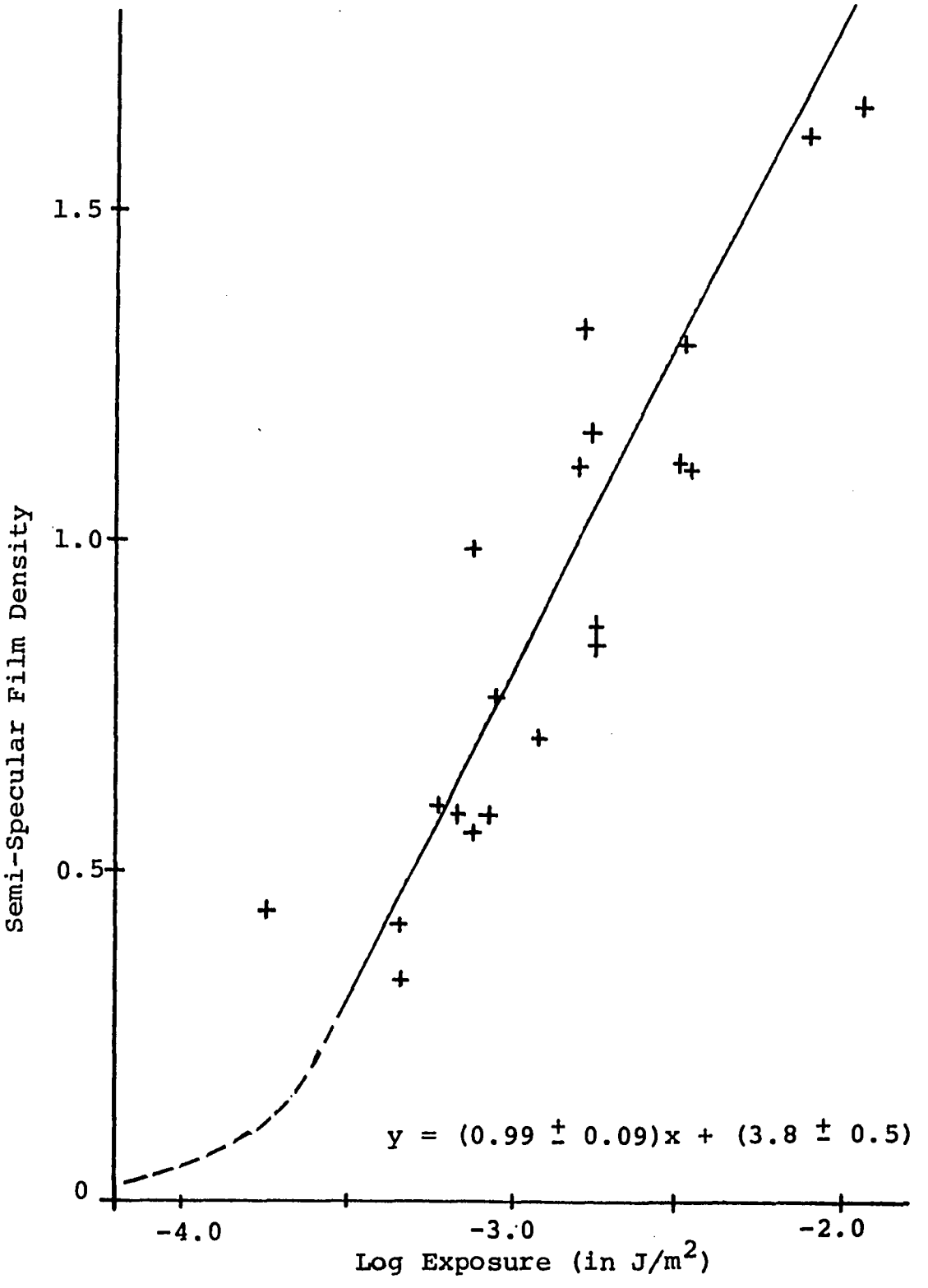

Figure 15

Seventy-five Nanosecond Characteristic Curve

The low power of the light passing through the narrow band pass filter prevented taking exposures at times shorter than the one-second setting on the shutter. Times greater than one second are of little interest here. After initially compiling a substantial amount of data at the one-second setting, it was necessary to calibrate the shutter time. This was done by removing film, diffuse filter, camera back, and all filters shown in Fig. 16. Placing the photodetector behind the camera with the oscilloscope at the most sensitive scale, it was then possible to get a measurable signal when opening and closing the shutter. This signal roughly resembled a square wave. Great care must be taken in performing this operation because a 1000 watt projector not only emits a great deal of visible light but it also projects large amounts of heat over a considerable distance. Shutter leaves are very thin and fragile; being black they readily heat up to excessive temperatures and warp. Such an incident will virtually destroy a shutter. During this experiment the author learned why it is best to calibrate fixed unknowns before an experiment. After having the shutter repaired and then carefully calibrated, the exposures with varying intensity were taken. The film handling techniques and measurements were carried out the same as for the laser exposures. The plot of film density vs log E is a typical H & D curve as can be seen in Fig. 17. It differs from the nanosecond H & D curves in its position on the log E axis and also its slope. This is a sign of reciprocity failure. The data used to determine this

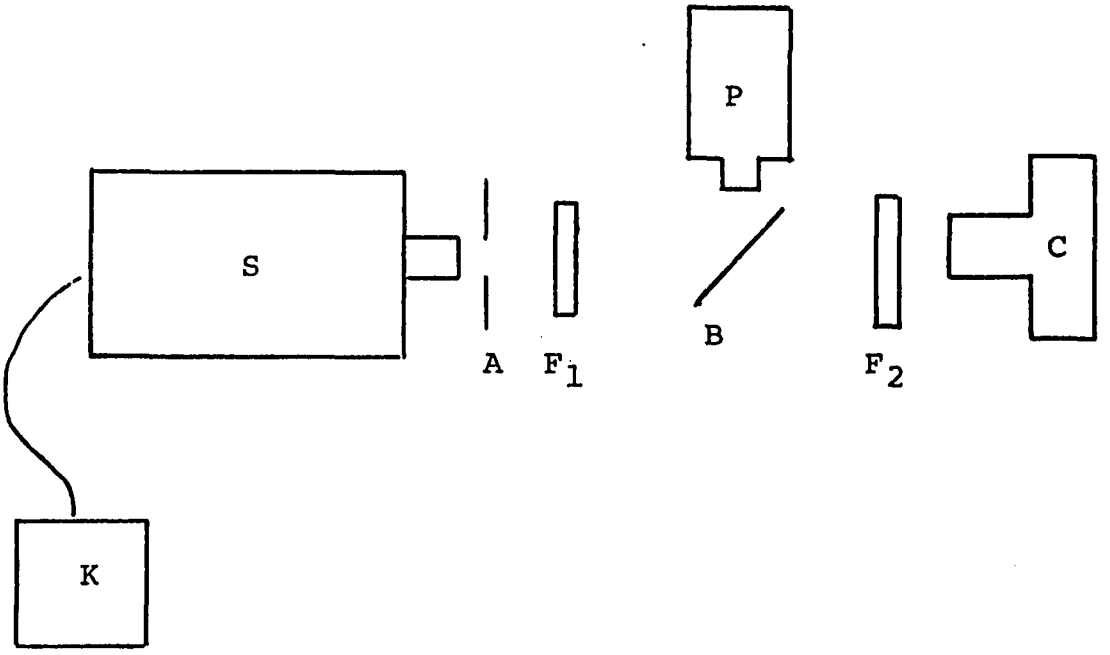

Figure 16

Apparatus for 1 Second Exposures

curve is presented in Table VII.

Out of all the data reported in this dissertation only that shown in Table VII and Fig. 17 is close to being comparable to any data previously reported. Kodak has gathered no data at nanosecond exposures but has reported a considerable number of 1 second curves in various publicity brochures.[16,17] These are spectral sensitivity curves and H & D curves along with contrast curves. There are different exposure spectra and develop parameters, and all are of course reported in terms of diffuse density. The author would hope that Kodak would have a curve with almost identical exposure and develop parameters as used here; however, that is not the case. There is an 800 nm monochromatic exposure at one second but it is developed with Kodak D-19.[18] There is also a D-76 developed daylight exposure at one second[19] (most likely with a Wratten filter No. 25 which Kodak suggests should always be used with this film and daylight exposures; however, it is not reported so). About the only thing that this author can determine from all of Kodak's data is that it is a complete maze of self-inconsistency. For example, if one determines γ (the slope of the D vs. log E curve) at 800 nm from the spectral sensitivity curves for the film developed with D-19 for 8 minutes at 68°F, it is found to be about 1.6.[20] But then when one determines from another brochure (exposed and developed as above), it is found to be approximately 2.4. Several more examples of self-inconsistency can be found in the two brochures, but will not be discussed here as it is irrelevant. Fig. 18 shows the 0.82

TABLE VII

One Second Exposure Data

Log Exposure (in $J/m^2 \pm 0.04$)	Film Density
-3.03	2.32 ± 0.02
-3.03	2.25 ± 0.02
-3.22	1.97 ± 0.02
-3.22	1.96 ± 0.02
-3.22	1.93 ± 0.02
-3.40	1.62 ± 0.01
-3.40	1.60 ± 0.01
-3.40	1.62 ± 0.01
-3.59	1.31 ± 0.01
-3.59	1.30 ± 0.01
-3.59	1.30 ± 0.01
-3.71	1.09 ± 0.01
-3.71	1.08 ± 0.01
-3.71	1.02 ± 0.01
-3.79	0.90 ± 0.01
-3.79	0.96 ± 0.01
-3.79	0.92 ± 0.01
-3.79	0.96 ± 0.01
-3.96	0.67 ± 0.01
-3.96	0.71 ± 0.01
-3.96	0.75 ± 0.01

Log Exposure (in $J/m^2 \pm 0.04$)	Film Density
-4.08	0.46 ± 0.01
-4.08	0.47 ± 0.01
-4.08	0.44 ± 0.01
-4.08	0.42 ± 0.01

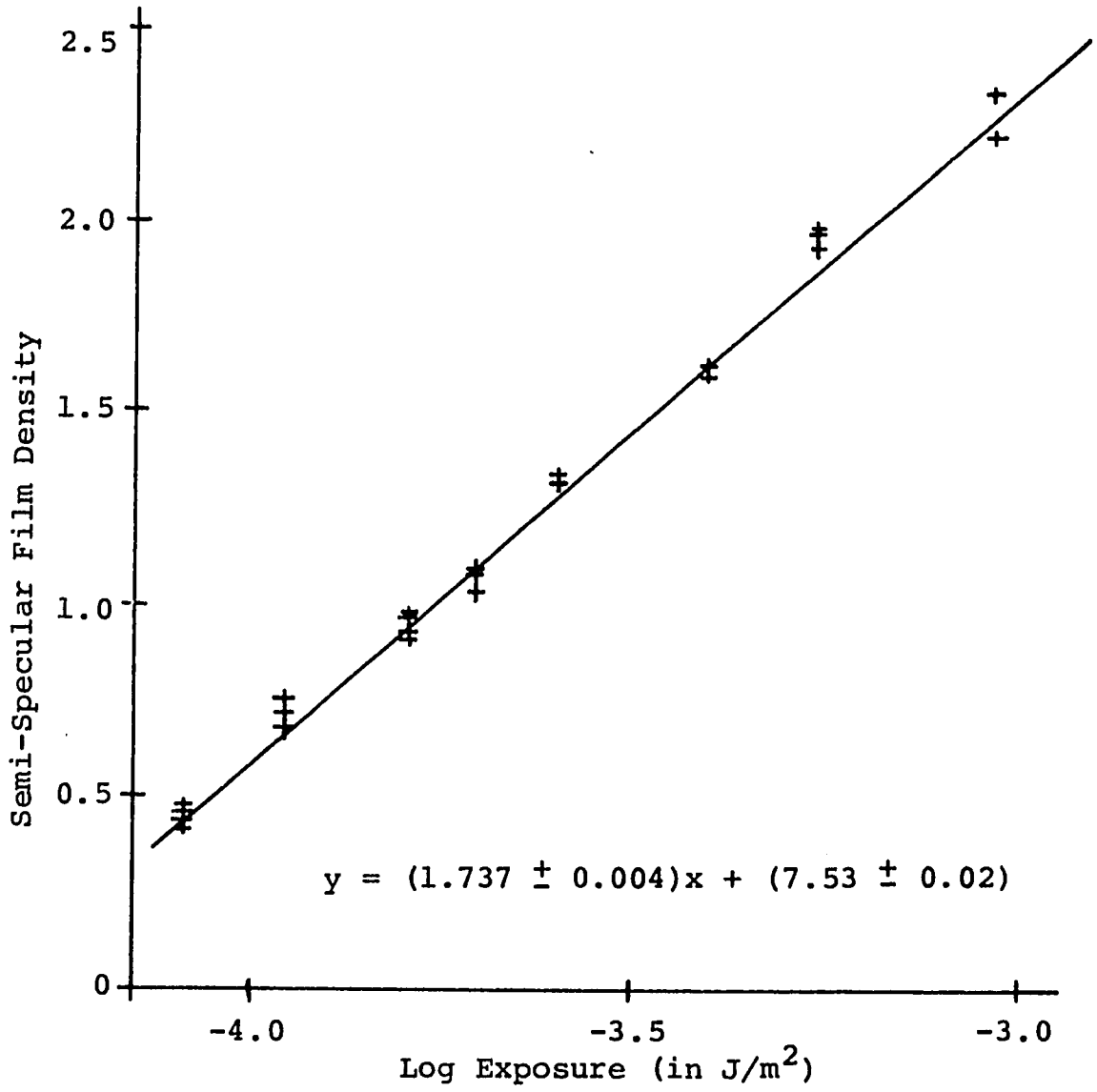

Figure 17

0.82 Second Characteristic Curve

second curve (A) from this paper together with the following Kodak curves:

(B) From a spectral sensitivity curve[21] of HIE421 film 4143 (which is the same emulsion as 2481 but on a thicker backing) developed in D-76 for 10 minutes at 68°F and exposed at a wavelength of 700 nm presumably for a time on the order of one second.

(C) From a characteristic curve (H & D curve)[22] developed with D-76 for 11 minutes at 68°F but exposed with daylight for one second.

Also for comparison the 19 ns curve from this paper is included (D). It is important to consider that curves A and D are reported in terms of 45° semispecular density while B and C are reported in terms of diffuse density. Also shown in Fig. 18 are diffuse density measurements from the same film used to produce spectral density curves A and D. The diffuse densities were measured on a non-scanning densitometer, Macbeth model #TD-504 (serial #1115) at Mostek Corporation, Carrollton, Texas. Really not very much can be concluded from Fig. 18. None of the four curves (A, A', B, and C) were obtained under exactly the same conditions. They also represent data from three different emulsion batches. This in itself may prohibit any comparison of absolute sensitivity. The contrast index, γ, or slope of A' is somewhat closer to B than C; however, its location along the log E axis places it closer to C. The parameters producing curve B are considerably closer to those producing curve A' than those producing curve C.

Another interesting point which should be noted in Fig. 18 is the slope of curve D (the nanosecond exposure

curve) is considerably lower than the slope of curve A. Thus one may conclude from this that there is more reciprocity failure with increased film blackening. This is consistent with the theories of the mechanics of reciprocity failure discussed in the appendix of this paper.

Curves showing the law of reciprocity or reciprocity failure are plotted as log E vs log I for a fixed film density. A typical reciprocity curve as actually measured and in part as predicted by theory is shown in Fig. 3 of the appendix. For two points on a horizontal part of the curve there is no reciprocity failure. On the other hand if two points of the curve do not fall on a horizontal then the law of reciprocity does not hold between those two exposure times. Using the H & D curves in Figs. 14, 15, and 17, a set of reciprocity curves each having three points can be plotted. Obviously it would be desirable to have more data, since a curve as complicated as a reciprocity curve is hardly determined by three points. A crude estimate of the location of the rest of the curve can be made from knowledge of other experimental work, together with the theory of the failure mechanism[23] (see appendix). Therefore the dashed lines in Fig. 19 are believed to resemble the family of correct curves for film densities of 0.2, 0.5, 1.0, and 1.5. In any case it is possible to conclude definitely that there is reciprocity failure between one second and 10^{-7} second exposures. The 20 and 80 ns data points are so close together and the uncertainty in the results enough, such that it is unfortunately not possible to

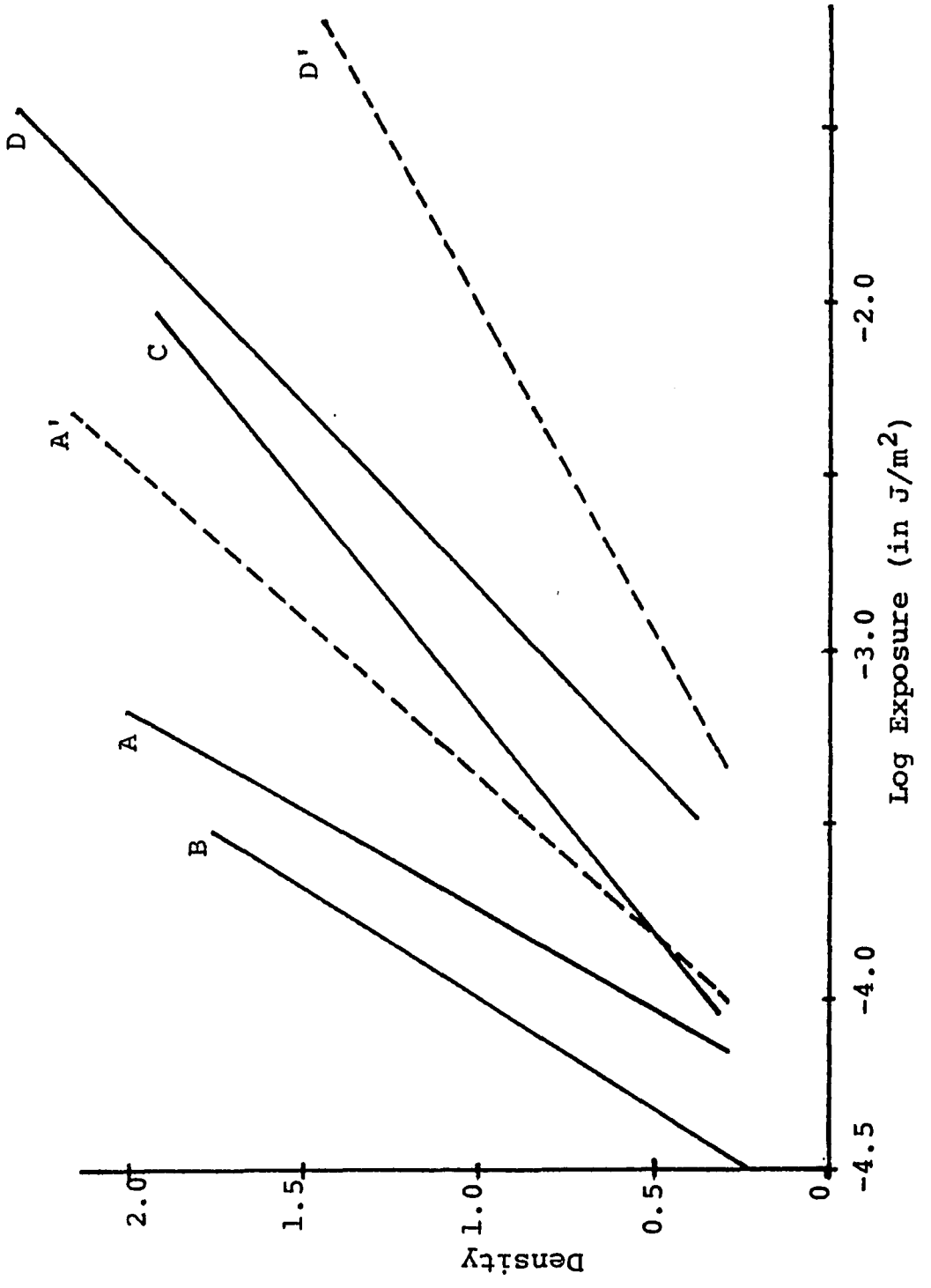

Figure 18

Comparison of Various Characteristic Curves

determine whether the slope is positive, negative, or zero. Thus this data neither proves nor disproves the Berg bend-over theory[24] (see appendix). The points are, however, close enough together along the log E axis that one may consider the sensitivity of Kodak HIE film to be a constant between 20 and 80 ns. This is of course very convenient. A quantitative estimate of laser power from film density data can be made from the data presented in this dissertation in any laboratory which possesses a Hughes-Nauman densitometer. Furthermore, a few exposures of the same film analyzed by anyone using other equipment would provide sufficient data to determine the relative collection efficiencies. Once the ratio between the blackening measured with their densitometer to that reported here is known for any one exposure time, that ratio may be used to calculate absolute intensities.

SUMMARY

The initial goal of this dissertation was to determine reliable techniques to make precision measurements of pulsed laser intensities. This was done in Chapter I, by statistical methods and large quantities of data. Then in Chapter II results were applied to a simple experiment which gives one another tool for making such measurements. In measuring photographic film reciprocity data, the film sensitivity in the laser pulse time domain is simultaneously determined. These data can in turn be applied to monitor laser pulse intensities and also laser stimulated pulse intensities. This procedure for monitoring intensities is much more practical

TABLE VIII

Reciprocity Data

Semispecular Film Density	Log Exposure (in J/m^2)	Log Intensity (in W/m^2)
	0.82 ± 0.01 second exposure time	
0.2	-4.12 ± 0.05	-4.21 ± 0.05
0.5	-3.95 ± 0.05	-4.04 ± 0.05
1.0	-3.66 ± 0.05	-3.75 ± 0.05
1.5	-3.38 ± 0.05	-3.46 ± 0.05
2.0	-3.10 ± 0.05	-3.18 ± 0.05
	75 ± 13 nanosecond exposure time	
0.2	-3.6 ± 0.2	3.5 ± 0.2
0.5	-3.3 ± 0.2	3.8 ± 0.2
1.0	-2.8 ± 0.2	4.3 ± 0.2
1.5	-2.3 ± 0.2	4.8 ± 0.2
2.0	-1.8 ± 0.2	5.3 ± 0.2
	19 ± 2 nanosecond exposure time	
0.2	-3.69 ± 0.04	4.03 ± 0.04
0.5	-3.37 ± 0.04	4.35 ± 0.04
1.0	-2.84 ± 0.04	4.88 ± 0.04
1.5	-2.31 ± 0.04	5.41 ± 0.04
2.0	-1.78 ± 0.04	5.94 ± 0.04

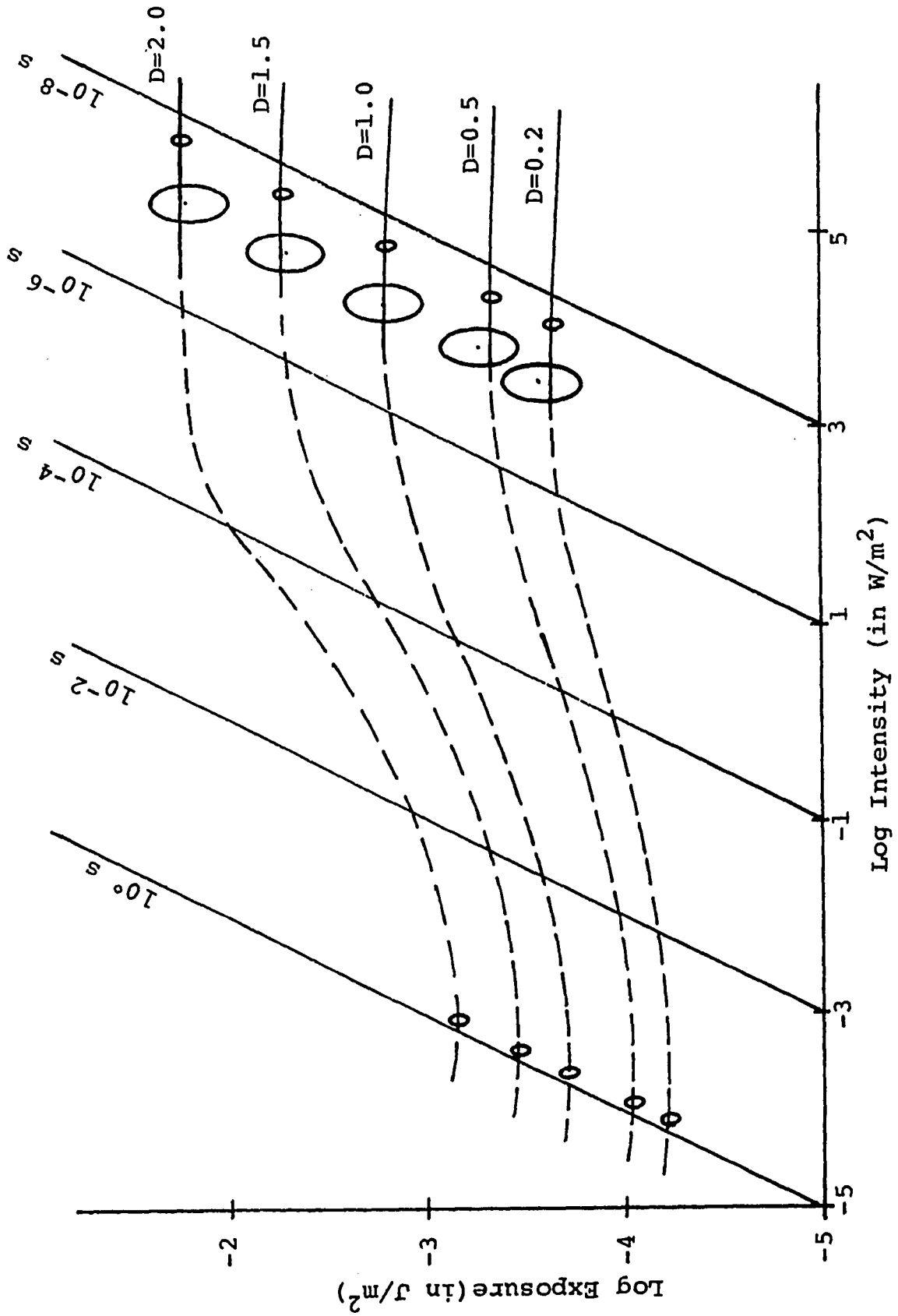

Figure 19

Reciprocity Curves

than the method used in Chapter I, as photographic film placed at the end of a spectrophotometer can be used to monitor a broad range of frequencies. Clearly one would need many photodetectors, strategically located, to measure the line intensities produced by a pulsed laser stimulated Raman spectrum. The difficulty in calibrating and geometrically placing several photodetectors would be prohibitive. One may well note at this time that the data in this dissertation determine reciprocity failure and film sensitivity only at 694.3 nm. This is true, but fortunately reciprocity failure is not wavelength dependent, other than considering that photons, not Joules, produce film blackening.[25] That is, one Joule of 694.3 nm photons is more effective in exposing film than one Joule of 690 nm photons, because it takes more 694.3 nm photons to produce one Joule of energy. One must also consider the spectral sensitivity of the film. Not all photons are equally effective at producing blackening. Films are more sensitive to some regions of wave-lengths than others because of the sensitizers added to the emulsion. The important thing to consider here is that there is very little difference in a spectral sensitivity curve at one second exposures and a spectral sensitivity curve at nanosecond exposures, other than a constant displacement along the log sensitivity (or y-) axis.[26] (This displacement is a result of the reciprocity failure between the two exposure times.) One may, with the data in Chapter II and a one second spectral sensitivity curve (for the appropriate developer and

develop parameters) determine the H & D curves at all wavelengths between 600 and 800 nm with considerable reliability.

One final note should be made here. The importance of precisely controlling all film develop parameters simply cannot be overemphasized. Photographic emulsions if properly handled can give quite precisely reproducible results. However, if any handling technique is done carelessly or without consideration for detailed controls, the results will be quite unsatisfactory.

PART II

A QUANTUM MECHANICAL PARADOX

INTRODUCTION

It is well known that there exists a fundamental limitation upon the precision which can be achieved in certain kinds of experimental measurements. This limitation, called the uncertainty principle, is a necessary consequence of quantum mechanics. In the interests of mathematical simplicity, we shall limit our consideration to isolated systems consisting of a single particle, constrained to move along the x axis of some Cartesian coordinate system. At any given time t, the particle will have a position x and linear momentum p_x. The uncertainty principle may then be stated as follows:

1. Any measurement of the quantity x at time t is subject to an uncertainty Δx^Q.

2. Any measurement of the quantity p_x at time t is subject to an uncertainty $\Delta p_x{}^Q$.

3. The product of Δx^Q and $\Delta p_x{}^Q$ (which we shall designate by the symbol U^Q) cannot be less than $h/4\pi$.

4. This conclusion is independent of the choice of the time t. The superscript Q refers to "quantum mechanics" and h is Planck's constant.

Suppose we inhabited a universe in which h had some value other than the present 7×10^{-34} J·s. In particular, suppose that h were zero. In such a universe, which we shall call the "Classical Universe", the uncertainty principle ought not

to impose any restriction on the precision of our measurements. The laws of classical mechanics (i.e., Newton's laws) ought to provide an adequate description of the motion of our hypothetical particle, and nothing in Newton's laws implies any fundamental limitations upon the precision which can be achieved in any experimental measurement. We therefore might imagine that $U^C = 0$. (The superscript C means "classical".) It is the purpose of this paper to develop a theoretical description of the motions of particles in certain isolated systems, within the framework of the laws of classical mechanics, which allows us to define and calculate the uncertainty product U^C in an apparently sensible fashion. We shall show that, in general, U^C so calculated is non-zero (the lack of a formal "Uncertainty Principle" notwithstanding), and indeed in some cases we shall be able to show that it is larger than the corresponding quantum uncertainty product U^Q.

This will lead us to the paradoxical conclusion that the introduction of the Uncertainty Principle into the laws of nature has made some things more certain than they would be without such a principle. Finally, we shall resolve this paradox by explaining the differences between the uncertainty introduced by quantum mechanics and that implied by classical mechanics.

QUANTUM MECHANICAL UNCERTAINTY

Schrödinger's formulation of quantum mechanics makes it obvious that the motions of particles in systems of atomic size

must be treated statistically. The solution $\Psi(t)$ of the wave equation,

$$\mathcal{H}\Psi = i\hbar\,(\partial\Psi/\partial t)_x \quad , \tag{1}$$

can be used to construct distribution functions for the positions of these particles. In particular, for one-dimensional, one particle systems, $\Psi^*(x,t)\Psi(x,t)dx$ is the probability that the particle will be located on a line segment of length dx, centered at x, at the time t. We assume that Ψ has been normalized, or that

$$\int_{-\infty}^{\infty}\Psi^*\Psi dx = 1. \tag{2}$$

If the system is in what is called a stationary state, the time dependence of Ψ^* will cancel that of Ψ so that the resulting distribution is solely a function of x.

Average values of various physical properties of the system can be calculated by means of the formula

$$\langle F\rangle^Q = \int_{-\infty}^{\infty}\Psi^*(x)\;\tilde{F}(x)\Psi(x)dx, \tag{3}$$

where $\tilde{F}$ is the operator corresponding to the desired property, F. We shall use this expression to calculate average values of x, x^2, p_x, and p_x^2.

The uncertainty principle may be stated most formally and precisely by means of the commutation relations which exist between operators corresponding to conjugate quantities, such as $\tilde{p}_x$ and $\tilde{x}$.

$$\tilde{x}\tilde{p}_x - \tilde{p}_x\tilde{x} = i\hbar. \tag{4}$$

From this expression, one can derive the relationship that we used to state the uncertainty principle in the introduction,

$$\Delta p_x^Q \Delta x^Q \geq h/4\pi, \tag{5}$$

if and only if we define Δp_x and Δx as the root-mean-square (standard) deviations of the quantities p_x and x from their respective mean values.[27]

$$\Delta x^Q = [\langle x^2 \rangle^Q - (\langle x \rangle^Q)^2]^{\frac{1}{2}} \tag{6}$$

$$\Delta p_x{}^Q = [\langle p_x{}^2 \rangle^Q - (\langle p_x \rangle^Q)^2]^{\frac{1}{2}} \tag{7}$$

Finally, we can calculate

$$U^Q = \Delta x^Q \, \Delta p_x{}^Q. \tag{8}$$

UNCERTAINTY IN CLASSICAL MECHANICS

Newton's laws do not give distribution functions for the positions of particles in systems describable by means of classical mechanics. Instead, one obtains equations of motion which enable one to locate all of the particles exactly at any instant of time. In particular, for a one-particle, one-dimensional system, x may be calculated exactly from

$$x = f(t). \tag{9}$$

The velocity of this particle may be calculated from the equation of motion as follows:

$$v(t) = (\partial x/\partial t)_x \, , \tag{10}$$

and, if relativistic effects may be neglected,

$$p_x = mv. \tag{11}$$

Nevertheless, one can still define a distribution function, W^C, for this system by asking "If I select a time of observation at random, what is the likelihood that I will encounter the particle?" The probability, W^C, of finding the particle on a line segment of length dx, centered at x, at

time t will be proportional to the amount of time spent by the particle in traversing the segment dx, inversely proportional to the length of the segment, and independent of the direction of travel (algebraic sign of v). In other words, W^C is inversely proportional to the speed, $|v|$. Further, we desire a distribution function which does not explicitly contain the time. We may invert the equation of motion to achieve

$$t = g(x). \tag{12}$$

By substituting g(x) for t in the expression for v(t), we obtain

$$W^C(x) = \frac{N}{|v(x)|} \tag{13}$$

The constant of proportionality can be obtained by normalization, just as it is in quantum mechanics.

$$\int_{-\infty}^{\infty} W^C dx = 1 \tag{14}$$

This distribution function may be used to calculate average values of various physical properties of the system, in a fashion similar to that employed in quantum mechanics;

$$\langle F \rangle^C = \int_{-\infty}^{\infty} W^C(x)\ F(x)\ dx \tag{15}$$

We shall use the above formula to calculate the average values of x, x^2, p_x and p_x^2, and to compute the standard deviations of the position and the momentum from their mean values, just as we did for the quantum mechanical distribution function, by means of

$$\Delta x^C = [\langle x^2 \rangle^C - (\langle x \rangle^C)^2]^{\frac{1}{2}}, \text{ and} \tag{16}$$

$$\Delta p_x^C = [\langle p_x^2 \rangle^C - (\langle p_x \rangle^C)^2]^{\frac{1}{2}}. \tag{17}$$

Then we can calculate

$$U^C = \Delta x^C \, \Delta p_x{}^C. \tag{18}$$

THE ONE-DIMENSIONAL HARMONIC OSCILLATOR: QUANTUM MECHANICAL TREATMENT

This system consists of two masses, m_1 and m_2 connected by a massless, frictionless spring of stiffness k, or by a single mass m suspended from an immovable support by means of such a spring. The equivalency of these two formulations of the problem is established when m is identified as the reduced mass:

$$m = m_1 m_2 / (m_1 + m_2). \tag{19}$$

The practical significance of this problem lies in the fact that vibrations of the nuclear framework of a molecule may be treated by considering that framework to be composed of a number of harmonic oscillators, with the effective fields produced by the bonding electrons serving as the springs. When such a system is set into oscillation along the spring axis, x, the resultant motion may be described as a linear superposition of motions obtained in stationary states. In both classical and quantum mechanics, a stationary state is characterized by a distribution function for the position of the particles which does not change spontaneously with time, plus the fact that the energy of the system is a constant of the motion. In neither case does it imply a lack of motion by the particles which compose the system. In quantum mechanics, the stationary state wave functions are given by

the following expression:

$$\Psi_n(x,t) = (\sqrt{\pi} x_o \, 2^n n!)^{-\frac{1}{2}} H_n(\frac{x}{x_o}) \exp\left[-\tfrac{1}{2}(\frac{x}{x_o})^2 + i(\Phi - \frac{2\pi E_n t}{h})\right]. \quad (20)$$

where

$$x_o = (2E_o/k)^{\frac{1}{2}} \quad (21)$$

and $H_n(\xi)$ is the n^{th}-order Hermite polynomial. The quantity Φ is an arbitrary constant phase factor. The states are numbered in order of increasing energy,

$$E_n = (n+\tfrac{1}{2})\frac{h}{2\pi}\sqrt{\frac{k}{m}} \, . \quad (22)$$

The distribution function,

$$\Psi_o^*(x,t)\,\Psi_o(x,t) = W^Q(x), \quad (23)$$

is plotted in Fig. 20.

In the above expressions, x is defined as the displacement of the spring from its equilibrium length.

We may use symmetry arguments to show

$$\langle x \rangle_n{}^Q = 0. \quad (24)$$

We can find $\langle x^2 \rangle_n$ with the aid of the recursion formula

$$\xi H_n(\xi) = \tfrac{1}{2} H_{n+1}(\xi) + n H_{n-1}(\xi). \quad (25)$$

The result is

$$\langle x^2 \rangle_n{}^Q = E_n/k \, . \quad (26)$$

The appropriate expression for the momentum operator is

$$\tilde{p}_x = i\hbar(\partial/\partial x)_t \, . \quad (27)$$

Symmetry arguments can be used to show

$$\langle p_x \rangle_n{}^Q = 0. \quad (28)$$

The average value p_x^2 is found with the aid of the relationship

$$\frac{d}{d\xi} H_n(\xi) = 2nH_{n-1}(\xi) \tag{29}$$

The answer is

$$\langle p_x^2 \rangle_n^Q = mE_n \ . \tag{30}$$

Finally, we may combine Eqs. (6), (7), (8), (24), (26), (28), and (30) to obtain

$$U^Q_n = E_n \sqrt{m/k} \ . \tag{31}$$

THE ONE-DIMENSIONAL HARMONIC OSCILLATOR: CLASSICAL MECHANICAL TREATMENT

The classical equation of motion for a one-dimensional harmonic oscillator in a stationary state is

$$x(t) = x_o \cos(\sqrt{k/m}\ t - \Phi). \tag{32}$$

As in the previous section, x is the displacement of the length of the spring from its equilibrium value and Φ is an arbitrary phase factor. We may substitute Eq. (32) into Eq. (10) to obtain an expression for the velocity v(t).

The kinetic and potential energies of the system convert sinusoidally into one another in such a way that their sum, the total energy E, is constant. The total energy may be computed by examining one of the points at which the kinetic energy (and therefore the velocity) is zero. At these values of x, called classical turning points, the potential energy V will then be the total energy. From this we can conclude

$$\therefore \ E = +\tfrac{1}{2}kx_o^2 \tag{33}$$

Equation (32) may be inverted, as suggested by the previous discussion leading to Eq. (12), to find the time as a function of position. The resultant expression may be substituted into the formula for v to yield:

$$v(x) = -\sqrt{\frac{2E}{m}}\left(1 - \frac{kx^2}{2E}\right)^{\frac{1}{2}}, \quad |x| \leq \sqrt{\frac{2E}{k}} \quad . \tag{34}$$

The restriction indicated on the allowed values of x is seen to be satisfied automatically by remembering that $\sqrt{\frac{2E}{k}}$ is the amplitude of the oscillation, x_o.

In the discussion leading to Eq. (13) we showed that the distribution function for the particle is inversely proportional to the absolute magnitude of the velocity, and gave the normalization condition for motion confined to the x axis. After performing the operations indicated in that section of this paper, we achieve

$$W^C(x) = \frac{1}{\pi}\sqrt{\frac{k}{2E}}\left(1 - \frac{kx^2}{2E}\right)^{-\frac{1}{2}} \tag{35}$$

This distribution function is displayed graphically in Fig. 21.

With the above distribution function the average values of x, x^2, p_x, and p_x^2 can be calculated as described previously. It is easily shown by symmetry arguments that

$$\langle x \rangle^C = 0 \tag{36}$$

and

$$\langle p_x \rangle^C = 0. \tag{37}$$

We can calculate, using Eqs. (15) and (35)

$$\langle x^2 \rangle^C = E/k \quad . \tag{38}$$

Similarly,

$$\langle p_x^2 \rangle^C = mE \tag{39}$$

Therefore the classical uncertainty product for the harmonic oscillator, from Eqs. (16), (17), (18), (36),(37), (38) and (39), is

$$U^C = E\sqrt{m/k} \ . \tag{40}$$

In comparing these results with the ones from the previous section it should be noted that the quantum mechanical energy, E_n, is limited to discrete integral multiples of $\sqrt{k/m}\ h/2\pi$, plus a certain irreducible minimum (zero-point) energy of half that amount. By way of contrast, the values of E allowed by classical mechanics form a continuum, and in particular, $E = 0$ is allowed. We can see, therefore, that the classical uncertainty may be arbitrarily small while the quantum uncertainty has a lower bound related to its zero point energy. Nevertheless, if we restrict ourselves in our selection of classical stationary states to those which happen to have energies equal to those permitted to the quantum mechanical stationary states, the quantum uncertainty is no greater than the classical uncertainty. This means that the outcome of an experiment designed to locate the position of the mass point m, performed at a randomly selected time, is no more predictable in a classical universe than a quantum one, provided that in both cases the oscillators are excited to stationary states of the same energy. The same thing can be said of experiments designed to measure the momentum. We note from Fig. 20 that the quantum mechanical "waviness" of the

mass point m has caused it to leak out of the region of the x axis to which it would have been confined in a classical universe; $\pm \sqrt{k/2E}$ are the classical turning points. This has the effect of broadening the distribution function beyond that found in classical mechanics (see Fig. 21) and therefore increasing the uncertainty in the position. On the other hand, the continuity requirements on Ψ causes the bulk of the remaining distribution function to pile up near the center ($x = 0$) where it makes a very small contribution to the second moment, $\langle x^2 \rangle$. This has the effect of localizing the electron to a greater degree than one would expect from the classical distribution function, because in the latter, probability density piles up at the classical turning points. The two effects (tunneling into the wings plus piling up near the center, relative to the classical distribution) evidently exactly cancel one another.

PARTICLE IN A ONE-DIMENSIONAL POTENTIAL WELL WITH INFINITELY STEEP WALLS (PARTICLE-IN-A-BOX): QUANTUM MECHANICAL TREATMENT

We next turn to another simple system, the particle in a box, or square-well-potential problem. This problem can be visualized physically in a classical universe by imagining a bead on a wire, the latter stretched between two unyielding walls. The wire is infinitely stiff, and the bead may slide back and forth without friction. Alternatively, one may imagine a bullet sliding freely in a pipe, the latter having an inner diameter just sufficient to permit passage of the

former, with both ends of the pipe welded shut. The usual quantum mechanical example is that of an electron travelling in the π-cloud of a conjugated (polyene) carbon chain of finite length. It may also be noted that this problem may be related to that of the harmonic oscillator by examining potential functions of the form

$$V_j(x) = k'(x/x_o)^{2j} \tag{41}$$

The harmonic oscillator is described by the above expression for $j = 1$ and the particle in a box by $j = \infty$.

The stationary state wave functions for the latter problem are

$$\Psi_n(x,t) = \begin{cases} (x_o)^{-\frac{1}{2}} \sin\left\{\frac{n\pi}{2}\left[1+\left(\frac{x}{x_o}\right)\right]\right\} \exp\left[i\left(\phi - \frac{2\pi E_n t}{h}\right)\right], & -x_o \leq x \leq x_o \\ 0, & |x| > x_o \end{cases} \tag{42}$$

The energies of these states are

$$E_n = n^2h^2/32m\ x_o^2\ , \tag{43}$$

and $2x_o$ is the length of the "box".

The complex square of the function in Eq. (42), with $n = 1$ and ϕ and $t = 0$, is plotted in Fig. 22.

In calculating $\langle x \rangle^Q$ and $\langle p_x \rangle^Q$, we shall discover that the integrands are always odd functions of x. Therefore,

$$\langle x \rangle_n^Q = 0 \tag{44}$$

$$\langle p_x \rangle_n^Q = 0 \tag{45}$$

The mean value of x^2 turns out to be

$$\langle x^2 \rangle^Q = \frac{x_o^2}{3} - \frac{h^2}{16\pi^2 m E_n}\ . \tag{46}$$

We can deduce $\langle p_x^2 \rangle^Q$ directly from the laws of quantum mechanics in this case because the energy of the system is totally kinetic. Because of that, the wave functions are eigenfunctions of the operator $\tilde{p}_x^2$ with eigenvalues $2mE_n$.

$$\therefore \langle p_x^2 \rangle^Q = 2mE_n \ . \tag{47}$$

Thence, from Eqs. (6), (7), (8), and (44)-(47),

$$U^Q = \left(\frac{2mE_n x_o^2}{3} - \frac{h^2}{8\pi^2} \right)^{\frac{1}{2}} \ . \tag{48}$$

PARTICLE-IN-A-BOX: CLASSICAL MECHANICAL TREATMENT

In classical mechanics, as in quantum mechanics, the energy for a system consisting of a particle in a one-dimensional box (making perfectly elastic collisions with the infinite potential walls) is totally kinetic. If the system is in a stationary state, the energy will be constant,

$$E = \frac{mv^2}{2} \ , \tag{49}$$

and therefore the magnitude of the velocity (though of course not the sign) will be constant, independent of x. Finally, the distribution function, which is inversely proportional to the magnitude of the velocity, will also be constant over the interval $-x_o < x < x$. After normalization, we find

$$\therefore \quad W^C = \begin{cases} 1/2x_o \ , & -x_o \leq x \leq x_o \\ 0 \ , & |x| > x_o \end{cases} \tag{50}$$

This function is plotted in Fig. 23.

Just as was the case in the quantum mechanical treatment of this problem, $\langle x \rangle^C$ and $\langle p_x \rangle^C$ will vanish because of the

odd symmetry of the integrand.

$$\langle x \rangle^C = 0 \tag{51}$$

$$\langle p_x \rangle^C = 0 \tag{52}$$

Next,

$$\langle x^2 \rangle^C = \frac{x_o^2}{3} \tag{53}$$

Just as was the case in the quantum mechanical treatment of the problem, the mean square momentum can be calculated directly from the energy.

$$\langle p_x^2 \rangle^C = 2mE \ . \tag{54}$$

We may calculate Δx^C, Δp_x^C, and U^C as before;

$$U^C = \left(\frac{2mEx_o^2}{3}\right)^{\frac{1}{2}} . \tag{55}$$

If we compare Eqs. (48) and (55) we note that the square of the classical uncertainty <u>exceeds</u> the square of the quantum one by an amount $h^2/8\pi^2$. It is easy to see why this must be so if we inspect Figs. 20-23. Beginning with the harmonic oscillator [particle in a parabolic potential well, $k'(x/x_o)^2$], we imagine a continuous deformation of the potential function in which the walls are made even steeper [particle in a general potential well, $k'(x/x_o)^{2j}$, $1 < j < \infty$]. Both the classical and the quantum distribution functions are gradually driven from their respective wings: probability density moves from the neighborhood of the classical turning points to the centers. In the limit of a well with infinitely steep walls [particle in a box, $\lim_{j \to \infty} k'(x/x_o)^{2j}$],

the classical distribution function loses its peaks at the turning points and completely flattens out. At the same time, the wings of the quantum distribution function which had previously extended beyond the turning points into the classically forbidden region (due to "tunneling" of the particle) become even more drastically damped. In the limiting case of the square-well potential, the classical and quantum distribution functions are both bounded by the classical turning points for the problem (i.e., the walls of the box). The peaking of the probability distribution in the neighborhood of the center of the box (which was displayed by the quantum mechanical harmonic oscillator wave function) is much less drastically affected by the deformation than its behavior at the wings; the former phenomenon is a relatively insensitive function of the slope of the walls. This peaking, in the case of the particle in the box, is no longer completely compensated by tunneling beyond the classical turning point. The quantum distribution is therefore obviously much more compact than the classical one for the particle in the box. The uncertainty in position, being a measure of the compactness of this function, is therefore less in quantum mechanics than in classical mechanics for a particle in a square potential well. To put it another way, in a quantum mechanical universe, the particle will probably be somewhere near the center of the box; in a classical mechanical universe, it could be anywhere in the box. It should be remembered here that our discussion is based upon the assumption that the quantum mechanical

particle is in its ground state, and the classical particle has been given an energy equal to the corresponding quantum mechanical particle for purposes of comparison.

RESOLUTION OF THE APPARENT PARADOX

At this point, some readers will very likely ask, "Where is the paradox? The author has artificially forced the classical particle into states with energies equal to those to which the quantum particle has been restricted by wave mechanics, and comparison of the resulting distribution functions is therefore meaningless. The author should have compared the distribution functions which result when both systems are in the states of lowest energy permitted by their respective systems of mechanics. In quantum mechanics, this state is forbidden to have zero energy because of the uncertainty principle. In classical mechanics, on the other hand, any energy including zero is allowed. Since U^C is always proportional to the energy, U^C will always be zero for the classical mechanical system. Since U^Q is always greater than zero, $U^Q > U^C$ for any system."

For readers who adopt this point of view, there is no rebuttal; it would be a waste of time for them to read further. For other readers, who believe that the comparison of systems at equal energies is appropriate and meaningful, we must look for a deeper cause for this apparent paradox, in order to resolve it.

This reason may be found by a reexamination of the distribution functions which we have developed to formulate the

problem. Suppose we were to obtain these distribution functions experimentally, rather than by means of a mathematical derivation from the theory. The experiments to be performed in both the classical and quantum mechanical universes would be the same. We should make many successive measurements of x, the position of particle in the system, noting the time of each measurement, t_j. We might perhaps by making a series of photographs of the system, illuminating with light of an appropriate wavelength (i.e., much smaller than the width of the distribution function $\sim 2x_o$). If the interval between successive photographs is made sufficiently small (i.e., much less than the orbital period h/E) we would be able to infer from these measured values of x the corresponding values of p_x, using the fundamental theorem of the differential calculus:

$$\frac{p_x(x_j)}{m} = \lim_{(t_{j+1} - t_j) \to 0} \left(\frac{x_{j+1} - x_j}{t_{j+1} - t_j} \right) \qquad (56)$$

From this ordered set of quantities, the experimentally measured x_j's and the derived p_j's, together with the corresponding time t_j, we should be able to infer the equation of motion for the particle, i.e., its orbit. As is well known, this scheme works well in ballistics and astronomy (portions of our "universe" which can be said to behave classically). It is also well known that this scheme fails utterly if used on systems of atomic size (the quantum universe) because the photons used to illuminate the system perturb the motions of the constituent particle in an unpredictable way. We can

express this mathematically as follows.

If we examine any classical equation for periodic motion, we shall discover that the location of a particle described by that equation depends upon the quantity $\Phi - 2\pi Et/h$, called the phase. The constant, Φ (initial phase), can be determined by specifying the initial condition of the system (the exact time the constituent particles were set into motion, and the method used to excite this motion). Once set into motion, the phase of a system in a stationary state remains in a linear function of time unless the system is disturbed. In classical mechanics, it is possible to make a position measurement in such a way as to leave the phase unchanged. Then, a subsequent measurement of position will yield the same result as one obtained had the first one not been made at all. Therefore, the ordering of the successive position measurements enables one to determine the equation of motion and predict the outcome of subsequent position measurements with great accuracy.

The same measurement, made upon a quantum mechanical system, produces an uncontrollable change in the phase constant Φ of the system. If we were to make photographs in this case, the ordering of successive ones is futile, because the positions measured correspond to different (unknown) values of Φ and one must know $\Phi_j - 2\pi Et_j/h$ to determine the orbits therefrom. One can make an analogy with the classical situation by imagining that some inept laboratory assistant dropped the ordered stack of photographs into a jumble on the floor

before he has marked upon them the corresponding times of observation, t_j. The principle inaccuracy in this analogy lies in the fact that in quantum mechanics, the "jumbling" of the photographs is automatic and unavoidable because it is produced by phase scrambling inherent in the measurement process. By way of contrast, in a classical universe, jumbling may easily be avoided simply by replacing the laboratory assistant responsible for it.

Finally, then, we may state the resolution of the paradox. In obtaining the classical distribution junction, we deliberately threw away information available to us (jumbled our data) by selecting observation times at random. In this way, we abandoned all hope of correlating the position of the particle with its phase and determining the orbit therefrom. Further, velocity information derived from such a jumble of observations will have no more than a statistical validity: the measured positions and the derived momenta can no longer be put into one-to-one correspondence. Therefore, one must be content to describe both positions and momenta by the widths of their respective distribution functions. Had we chosen to record the phases (by not selecting observation times at random) we could have determined orbits exactly and therefore determined position and momenta simultaneously with arbitrary accuracy. In quantum mechanical systems, the phase is automatically and unpredictably changed during each act of measurement, so that positions and momenta may never be put into one-to-one correspondence. In other words, $U^C > 0$ is

the consequence of the laws of physics; $U^C > 0$ is apparently the consequence of some combination of laziness, stupidity or obstinance on the part of the experimenter.

Before leaving this subject, let us qualify the statement that $U^C > 0$ implies some scientific or moral defect in the measurer of x and p_x. Suppose, in the hypothetical classical mechanical universe described above, that atoms were as small and as numerous as they are in our own quantum mechanical universe. The fact that one could, in principle, make phase measurements on Avagadro's number of particles does not mean that it would be practical to do so. One might be content, therefore, to describe the behavior of matter by means of the physical properties obtained by averaging over a large ensemble of identical systems, with no guarantee that there would be any correlation between the phases of various members of this ensemble. It is understood here that we refer to a microcanonical ensemble; the constituent systems can exchange neither matter nor energy.

If we are so content, it is a fundamental hypothesis of statistical mechanics that the averages calculated from successive measurements at random times on an individual system will be the same as averages calculated from a simultaneous measurement upon a large number of systems identical to the first, such systems having uncorrelated phases. This means that U^C, as calculated in the previous sections of this paper, may be an appropriate measure of the precision with which measurements can be made in practice upon a microscopic

ensemble of isolated atomic-sized systems in a classical universe. This uncertainty, however, is the result of a phase scrambling produced by the process of ensemble averaging rather than by fundamental limitations imposed by the laws of nature on the properties of microscopic systems. In a quantum mechanical universe, phase scrambling is complete at the microscopic level; ensemble averaging produced no further increase in the uncertainty, so that U^Q is an appropriate measure of the precision with which measurements can be made at either the microscopic or macroscopic level.

ACKNOWLEDGEMENT

We wish to thank Professor D. K. Carpenter for helpful discussions.

Captions for Figures 20, 21, 22, 23

Fig. 20 Quantum Mechanical distribution function for a one-dimensional harmonic oscillator in the stationary state of lowest energy state, E_o. The corresponding turning points in classical mechanics are $\pm x_o$. The distribution function is represented by the hatched area; the potential energy by the heaviest curve.

Fig. 21 Classical Mechanical distribution function for a one-dimensional harmonic oscillator excited to the same energy, E_o, as that of the corresponding quantum mechanical state of lowest energy. The turning points are $\pm x_o$. The distribution function is represented by the hatched area; the potential energy by the heaviest curve.

Fig. 22 Quantum Mechanical distribution function for a one-dimensional particle-in-a-box in the stationary state of lowest energy, E_1. The corresponding turning points in classical mechanics are $\pm x_o$. The distribution function is represented by the hatched area; the potential energy by the heaviest curve.

Fig. 23 Classical Mechanical distribution function for a one-dimensional particle-in-a-box excited to the same energy state, E_1, as that of the corresponding quantum mechanical energy state of lowest energy. The turning points are $\pm x_o$. The distribution function is represented by the hatched area; the potential energy by the heaviest curve.

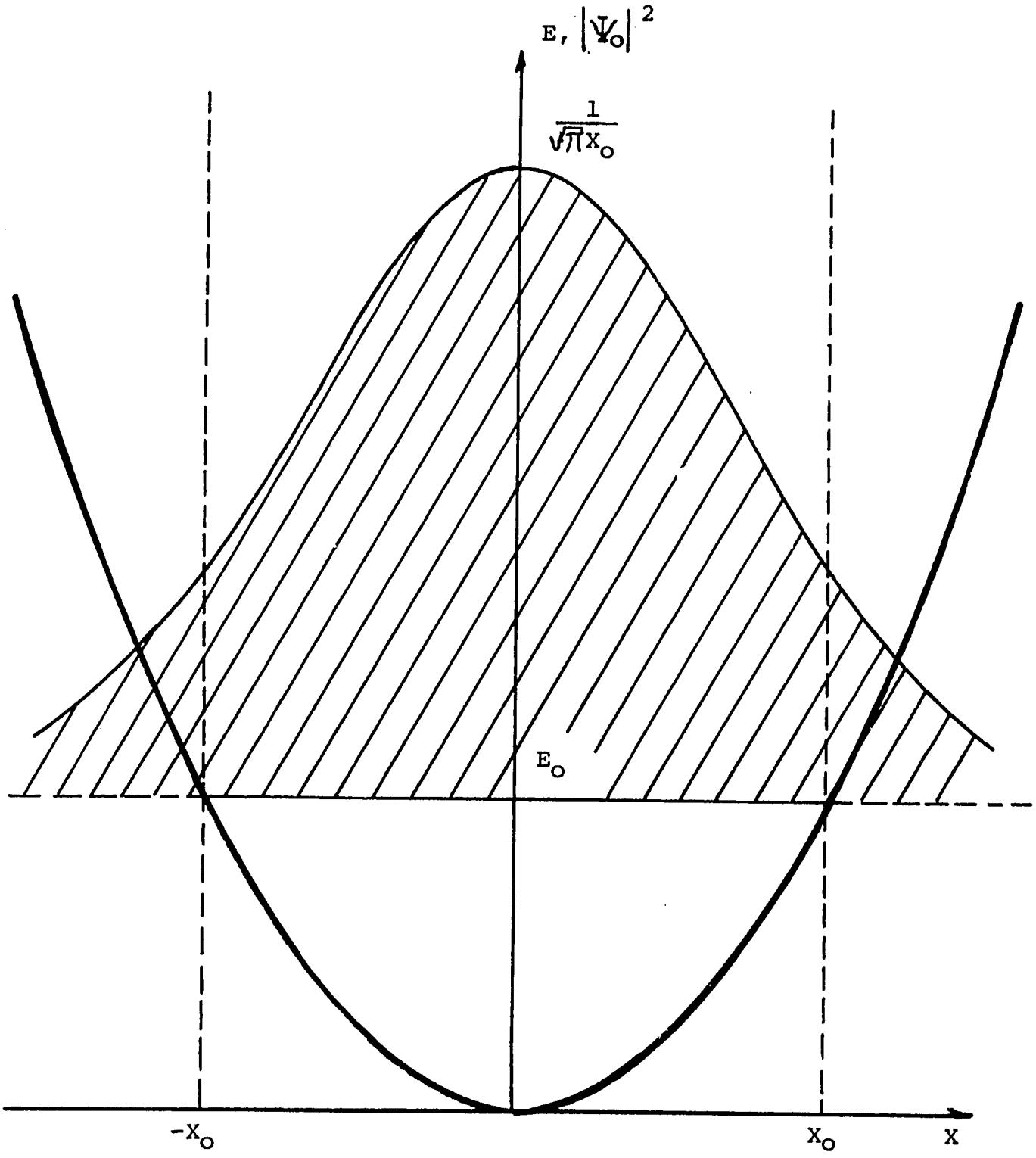

Figure 20

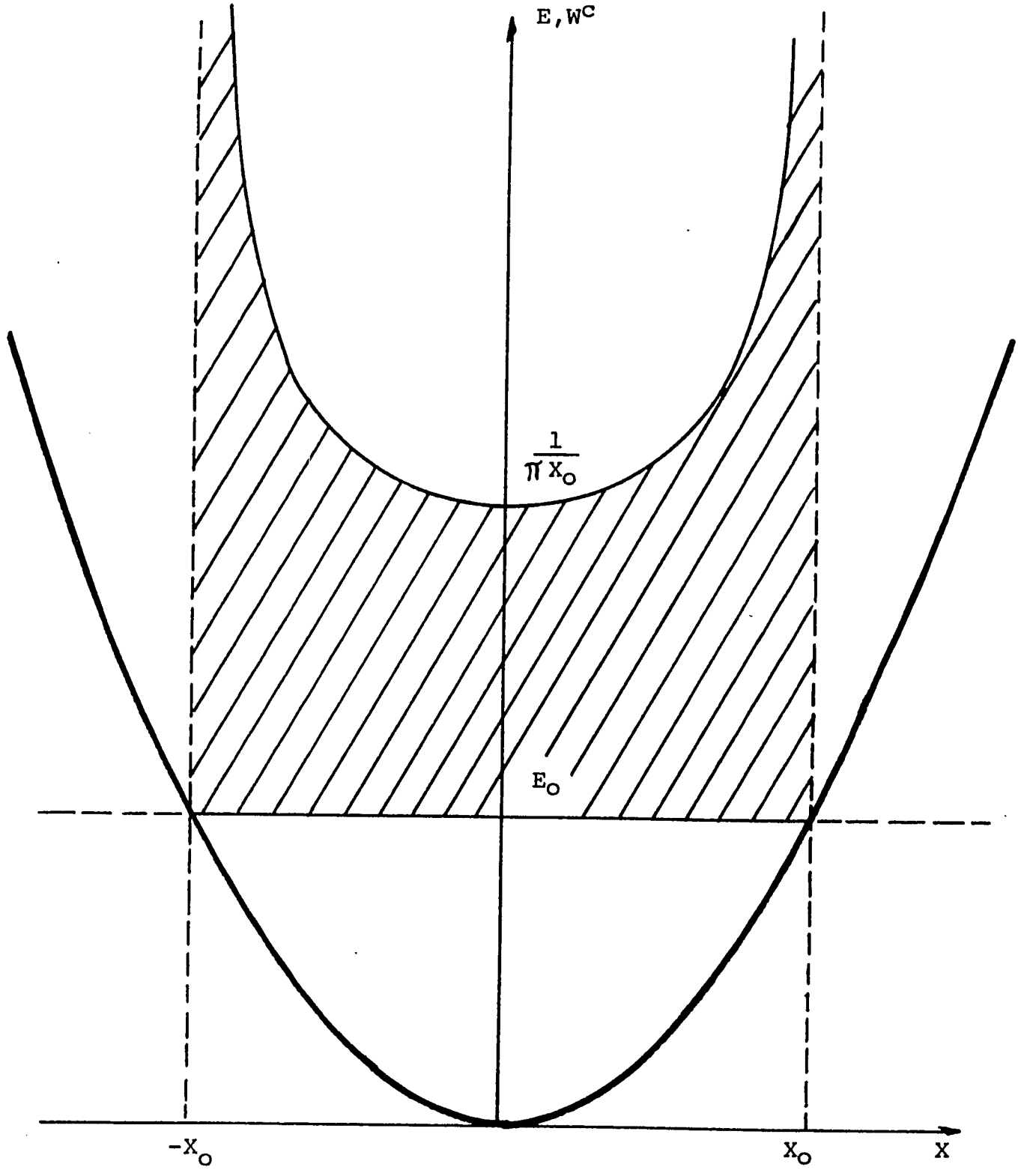

Figure 21

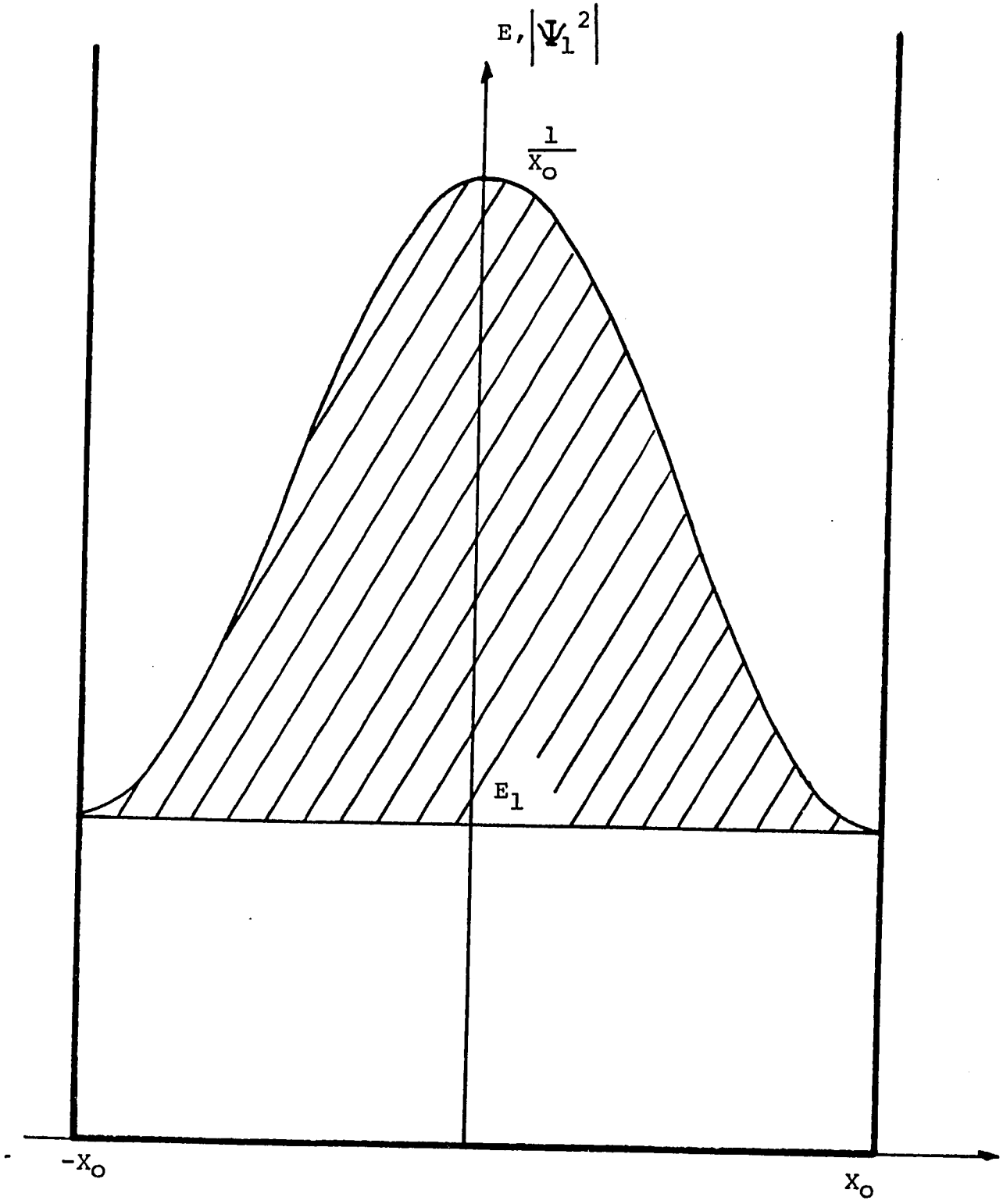

Figure 22

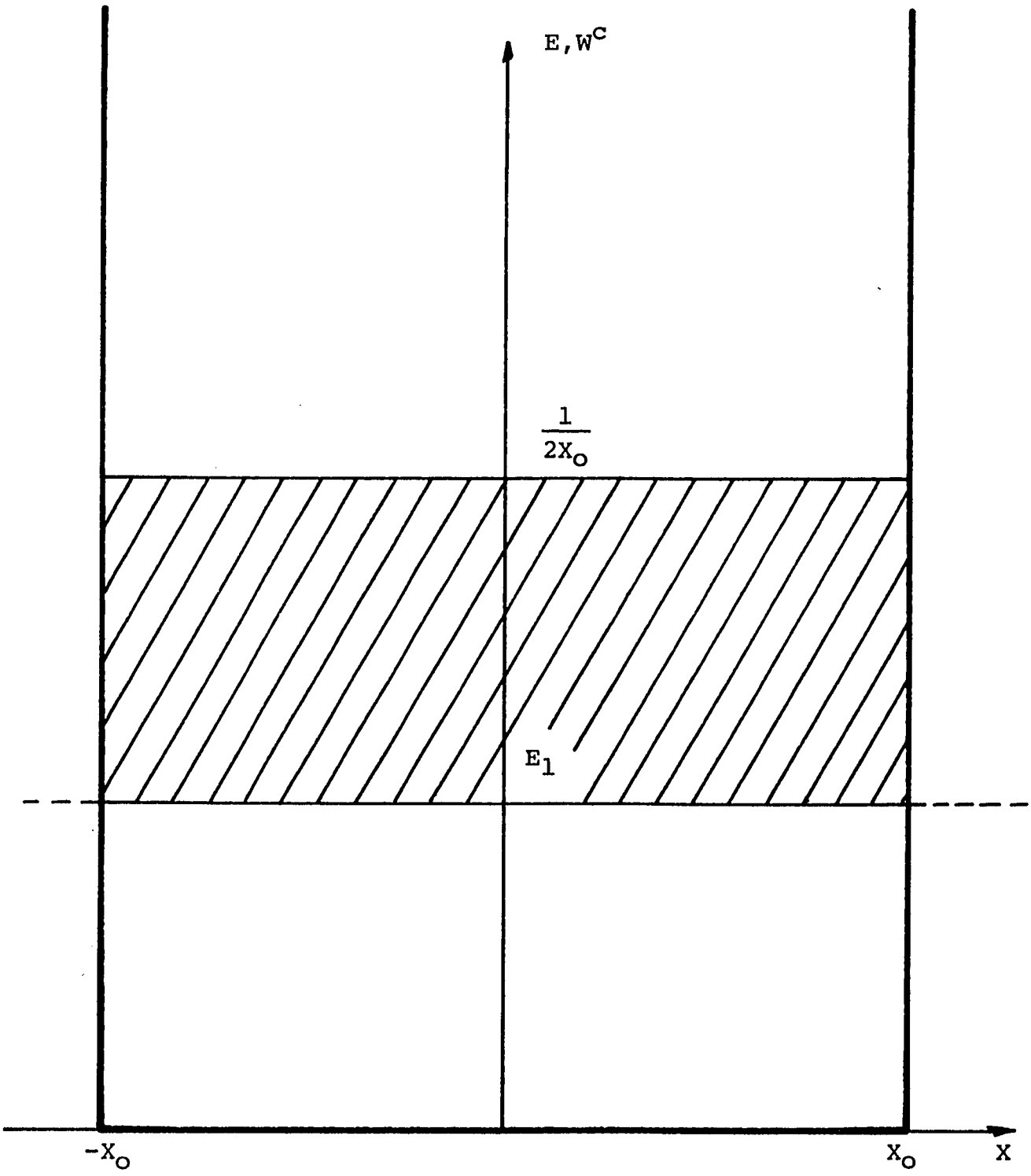

Figure 23

REFERENCES

[1] V. Evtuhov and J. K. Neeland, "Pulsed Ruby Lasers" in Lasers, Vol. 1, edited by A. K. Levine (Marcel Dekker, Inc., N. Y., 1966) Chap. 1.

[2] M. Born and E. Wolf, Principles of Optics, 4th ed., (Pergamon Press, Oxford, 1970) p. 63 ff.

[3] R. W. Hellwarth, "Q Modulation of Lasers" in Lasers, Vol. 1, edited by A. K. Levine (Marcel Dekker, Inc., N. Y., 1966) Chap. 4.

[4] B. Soffer, J. Appl. Phys. 35, 2551 (1964).

[5] R. A. Hollier and J. D. Macomber, Appl. Optics 11, 1360 (1972).

[6] R. A. Hollier and J. D. Macomber, J. Appl. Phys. 45, 2923 (1974).

[7] E. Garmire, private communication.

[8] Born and Wolf, op. cit., p. 63 ff.

[9] H. D. Young, Statistical Treatment of Experimental Data (McGraw-Hill Book Co., Inc., N. Y., 1962).

[10] R. W. Bunsen and H. E. Roscoe, Ann. Physik Chem, 117, 529 (1862).

[11] M. Hercher and B. Ruff, J. Opt. Soc. Am., 57, 103L (1967).

[12] C. E. K. Mees and T. H. James, The Theory of the Photographic Process, 3rd ed. (Macmillan, N. Y., 1966), p. 144.

[13] Elvin Hughes, Jr. and Robert V. Nauman, U. S. Pat. #3,751,171, Aug. 7, 1973, "Apparatus for Adapting a Spectrophotometer to Perform the Function of a Densitometer."

[14] Kodak Plates and Films for Science and Industry, first ed., 3rd printing (Eastman Kodak Co., 1967), p. 30.

[15] Ibid.

[16] Ibid.

[17] Kodak Infrared Films bulletin N-17, (Eastman Kodak Co., 1971).

[18] Kodak Plates, op. cit., p. 14d.

[19] Kodak Infrared, op. cit., p. 10.

[20] Kodak Plates, op. cit., p. 14d.

[21] Kodak Infrared, op. cit., p. 12.

[22] Kodak Plates, op. cit., p. 15d.

[23] Mees, op. cit., Chap. 19.

[24] Ibid., p. 138.

[25] Ibid., Chap. 19.

[26] Loc. cit.

[27] E. Merzbacher, Quantum Mechanics, (John Wiley and Sons, Inc., N. Y., 1965), pp. 154-155.

[28] R. W. Gurney and N. F. Mott, Proc. Rev. Soc. (London) Ser. A, 164, 151 (1938).

[29] Mees, op. cit., p. 103.

[30] Ibid., p. 109.

[31] Ibid., p. 138.

[32] Ibid., p. 109.

[33] Ibid., p. 138.

[34] N. F. Mott and R. W. Gurney, Electronic Processes in Ionic Crystals, 2nd ed., (Oxford U. Press, N. Y., 1948), Chap. 7.

[35] E. A. Baker, J. Phot. Sci., 4, 101 (1956).

[36] G. Sprague, J. Appl. Phys. 32, 2410 (1961).

[37] B. E. Bayer and J. F. Hamilton, presented at the Colloq. Intern. Sci. Fot., Sept. 23-28, 1963, Turin, Italy.

[38] Mees, op. cit., p. 138.

[39] Ibid., p. 109.

[40] Ibid., p. 138.

[41] J. H. Webb, J. Opt. Soc. Am., 23, 316 (1933).

[42] M. Biltz and J. H. Webb, J. Opt. Soc. Am., 38, 561 (1948).

[43] Mees, op. cit., p. 141.

[44] Ibid., p. 139.

APPENDIX

The Theory of the Formation of Latent Images, and of the Failure of the Reciprocity Law, in Photographic Emulsions

In order to explain the cause of high intensity reciprocity failure, it is necessary to present a brief explanation of how the latent image is formed in a photographic emulsion. Such an emulsion consists of a gelatin containing microscopic grains of silver halide crystals which usually have been made impure by the addition of an amount of another silver halide. These impurities cause defects in the crystal lattice which may serve as shallow trapping centers. In fact, the edges of the grains themselves are defects in the crystal lattice causing the surface of the grain to have a very large number of trapping centers. Now consider what happens when a photon strikes a grain. An electron in the valence band of the crystal may absorb the energy of the photon and be excited to the conduction band, leaving a hole in the valence band, as shown in Fig. 24.

The free electron then moves about the crystal until it is either recaptured by a hole or captured by a trapping center where it is temporarily localized, as shown in Fig. 25(a). The trapped electron may either escape and move to another trap or a hole, or it may remain in the trap long enough for a mobile silver ion to be captured by the trapped electron

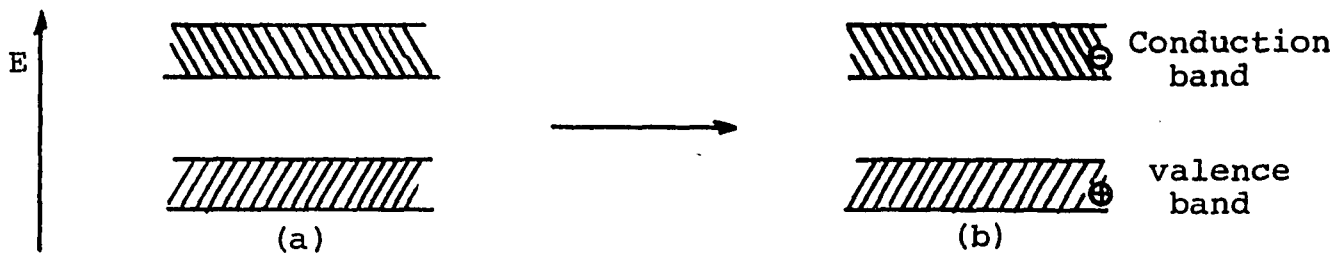

Figure 24

Photon Excitation

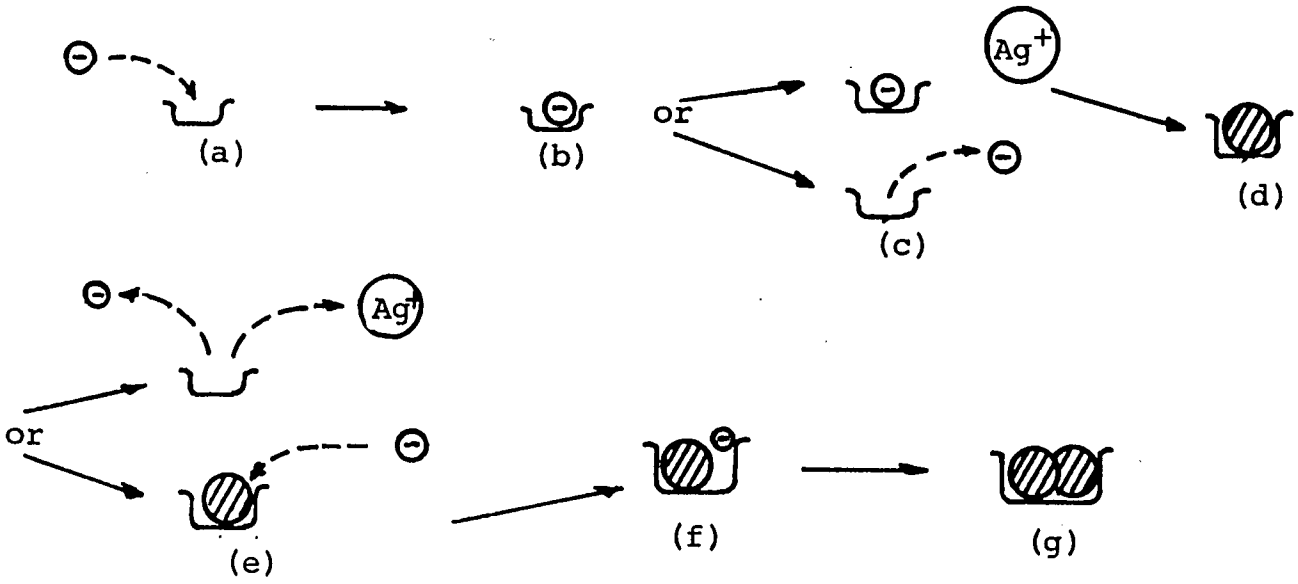

Figure 25

Exposure Mechanism

forming an unstable atom, Fig. 25(d). The silver atom will in time decompose back into a silver ion and an electron unless the atom which also is a trapping center captures another free electron [Fig. 25(e)] and a second silver ion [Fig. 25(f)] forming a stable two-atom speck [Fig. 25(g)]. This process may of course continue forming a larger speck, and at any time an atom in the speck may decompose back into a silver ion and an electron. A one-atom speck, as mentioned previously, is unstable; a two-atom speck is quite stable, having a mean lifetime of several days. In fact, as more atoms are added to the speck, it becomes increasingly more stable. The preceding mechanism is called the modified Gurney-Mott theory.[28] Another theory due to Mitchell[29] simply has the cation arriving at the trapping center first, then the electron. Berg[30] has calculated the mean time for the ionic step, i.e., the trapping of the silver ion [Fig. 25(b) to 25(d)], for the various trapping centers involved in the two mechanisms. Upon comparing these values with experimentally obtained information, it would seem that the Gurney-Mott theory is the better of the two.

A short note now must be made on the development probability of a grain containing one or more silver specks. It has been shown[31] that a grain containing one four-atom speck has about a 50-50 chance of being developed. A single larger speck leads to a higher development probability and a single smaller speck leads to a smaller development probability. It has also been shown[32] that a grain containing n

silver atoms distributed over several small specks is less likely to be developed if all of the n atoms were contained in a single large speck.

There are four processes[33] which have been proposed to explain high intensity inefficiencies. They are: (1) ionic limitation, (2) competitive nucleation, (3) recombination effects, and (4) topographic effects. The appendix paper has presented enough fundamentals of image formation to discuss three of the processes. For the sake of brevity the fourth process will not be considered here.

(1) Ionic Limitation

The charge on a silver speck will build up as electrons are trapped unless silver ions are added at the same rate. This is not possible if the electrons are arriving at the speck at a rate greater than τ_n, the ionic step mean life. Therefore after the charge has reached the limit that the speck can trap, new electrons arriving at the trap will be repelled by coulombic interactions. The excess electrons will then move to other trapping sites forming several smaller specks rather than one large one. This, as was stated previously, is not as effective in developing the grain. This process was proposed by Mott and Gurney.[34]

(2) Competitive Nucleation

This process which was considered by Baker[35] and by Sprague[36] and also Bayer and Hamilton[37] is similar to the ionic limitation. A high intensity exposure releases a large number of electrons; if the nucleation probability is

high compared with the growth probability, then many two-atom specks will be formed. Nucleation is defined as pairs of electrons combining at a trap followed by migration of two silver ions to the trap to form stable two-atom nuclei.

(3) Recombination Effects

The recombination of an electron with a hole would be expected to follow second order kinetics, since the probability would be proportional to the product of the number of holes and the number of electrons. Mechanisms leading to the formation of a silver atom would follow lower order kinetics. Because of this a high intensity exposure increases the probability of recombination at a faster rate than a mechanism leading to a silver atom.

Probably no <u>one</u> of the above processes is totally responsible for high intensity reciprocity failure, but rather a combination of all the processes is going on simultaneously.

It is assumed that the mean life of the electron is negligibly short[38] compared to the mean life of the ionic step T_n which Berg has calculated to be on the order of 10^{-6} seconds.[39] If the exposure is in fact "so short that all of the electrons are released before any one of them has been trapped and neutralized, the high-intensity inefficiency reaches the greatest possible value and further reduction of the exposure time would introduce no additional loss of sensitivity."[40] Thus there is an increasing inefficiency in the reciprocity curve until the exposure is on the order of 10^{-6} seconds. When the exposure time is equal to the

life-time of the ionic step, the inefficiency is a maximum and the reciprocity curve bends over becoming horizontal for shorter exposures (see Fig. 26). This is called the Berg bend-over point.

Since many photographic properties depend on the wavelength of the incident light, temperature, and the developing procedure, it is important to consider the effects of these on reciprocity failure. Extensive experimental work by Webb[41] and by Biltz and Webb[42] has shown that the shape of the reciprocity curve is substantially independent of wavelength. However, there is a diagonal shift in the curve along the lines of constant t. This is to be expected since the rate of absorption of quanta at the optimum remains the same. Since the major steps in the formation of the latent image are thermally activated, the mean life of these steps increases with decreasing temperature. This essentially causes a horizontal shift to the left in the reciprocity curve (Fig. 27). In fact, at very low temperatures, the mean life of the ionic step may become so long that the Berg bend-over point would be moved so far to the left that reciprocity failure would not even be observed over the usual intensity range. Note that the -186°C curve is parallel to the log I axis. If it is desired to use photographic plates for quantitative work, it is necessary to eliminate all development variables, since the density of the film and the reciprocity curves do not vary linearly with these variables. In particular increasing the developing time t_k reduces high

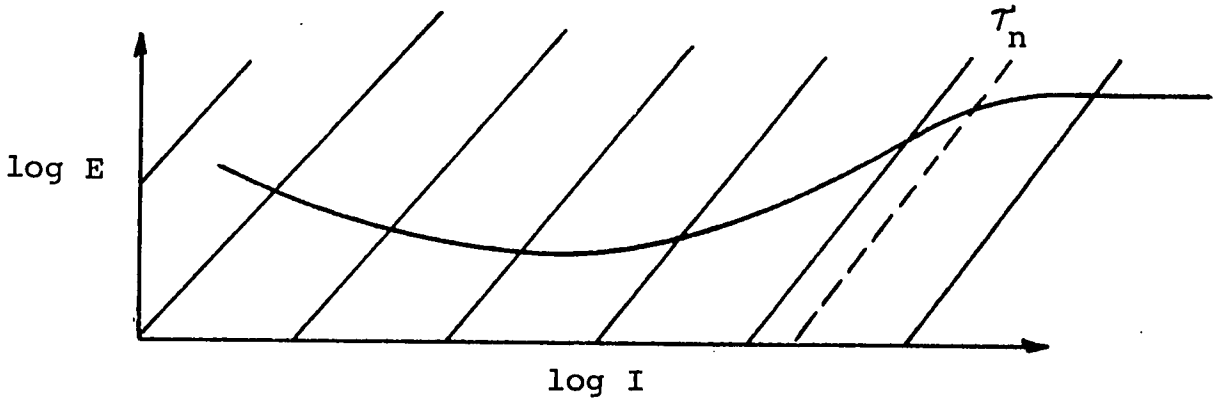

Figure 26

A Typical Reciprocity Curve

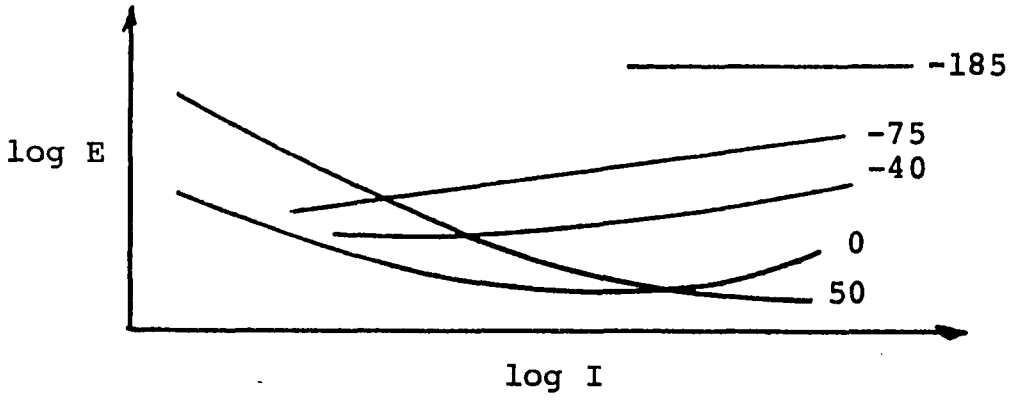

Figure 27[43]

Temperature Dependence of Reciprocity Failure

intensity reciprocity failure (Fig. 28). Besides using the same developing time, it is necessary to use the same kind of developer, the same agitation, and film from the same emulsion batch. The film should be developed as soon as reasonably possible after exposure in freshly prepared developer.

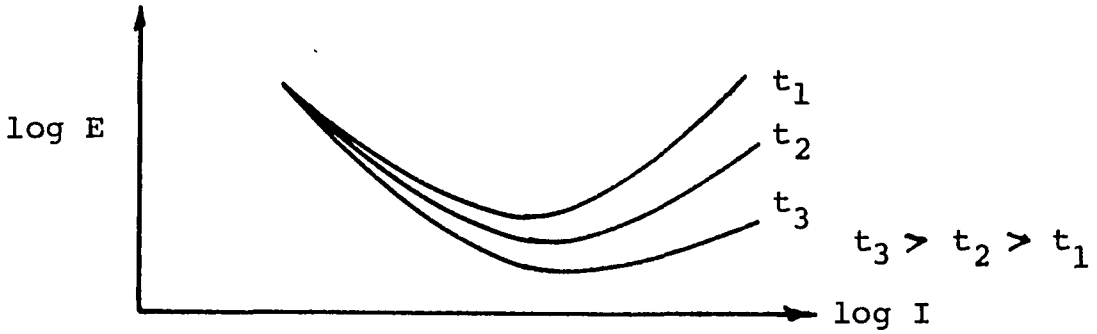

Figure 28[44]

Develop Temperature Dependence of Reciprocity Failure

VITA

Rory Oliver Rice was born in Baton Rouge, La., on February 10, 1946. He is the younger son of Mr. and Mrs. Richard S. Rice of that city. He is married to the former June Delambre of Baton Rouge, who also holds a degree from L. S. U. in Home Economics.

The only schooling he has ever known after the first grade has been on the L. S. U. campus, having graduated from University High in 1964, and having received a B. S. degree in chemistry from L. S. U. in 1968.

He immediately started post-graduate work toward a doctorate degree in physical chemistry, completing his classroom work in 1973. During most of this period he served as lab instructor in the chemistry department.

On January 1, 1974, he accepted a position with Mostek Corporation in Carrollton, Texas, where he is presently employed. He and his wife make their home in nearby Irving, Texas. During that year he completed work on this dissertation and in April, 1975, successfully passed his oral examination. He is being awarded a Doctor of Philosophy degree in physical chemistry from Louisiana State University on May 16, 1975.

EXAMINATION AND THESIS REPORT

Candidate: Rory Oliver Rice

Major Field: Chemistry

Title of Thesis: I. Precision Measurements with a Ruby Laser and II. A Quantum Mechanical Paradox

Approved:

James Dale Macomber
Major Professor and Chairman

James R. Trayham
Dean of the Graduate School

EXAMINING COMMITTEE:

Date of Examination:

April 4, 1975